HHS Public Access

Author manuscript

Cell Rep. Author manuscript; available in PMC 2020 July 13.

Published in final edited form as:

Cell Rep. 2020 June 23; 31(12): 107782. doi:10.1016/j.celrep.2020.107782.

NeuroD1 Dictates Tumor Cell Differentiation in Medulloblastoma

Yan Cheng[1,4], **Shengyou Liao**[5], **Gang Xu**[1], **Jian Hu**[1,4], **Duancheng Guo**[4], **Fang Du**[1], **Alejandra Contreras**[2], **Kathy Q. Cai**[1], **Suraj Peri**[3], **Yuan Wang**[4], **David C. Corney**[6], **Anne Marie Noronha**[6], **Lianne Q. Chau**[7], **Ginger Zhou**[6], **David L. Wiest**[2], **Alfonso Bellacosa**[1], **Robert J. Wechsler-Reya**[7], **Yi Zhao**[5], **Zeng-jie Yang**[1,8,*]

[1]Cancer Biology Program, Fox Chase Cancer Center, Temple University Health System, Philadelphia, PA, USA

[2]Blood Cell Development and Function, Fox Chase Cancer Center, Temple University Health System, Philadelphia, PA, USA

[3]Biostatistics and Bioinformatics Research Facility, Fox Chase Cancer Center, Temple University Health System, Philadelphia, PA, USA

[4]Laboratory of Molecular Neuropathology, College of Pharmaceutical Sciences, Soochow University, Suzhou, China

[5]Bioinformatics Research Group, Chinese Academy of Sciences, Beijing, China

[6]Genomics and Molecular Genetics, GENEWIZ Co., South Plainfield, NJ, USA

[7]Tumor Initiation& Maintenance Program, Sanford Burnham Prebys Medical Discovery Institute, La Jolla, CA, USA

[8]Lead Contact

SUMMARY

Tumor cells are characterized by unlimited proliferation and perturbed differentiation. Using single-cell RNA sequencing, we demonstrate that tumor cells in medulloblastoma (MB) retain their capacity to differentiate in a similar way as their normal originating cells, cerebellar granule neuron precursors. Once they differentiate, MB cells permanently lose their proliferative capacity and tumorigenic potential. Differentiated MB cells highly express NeuroD1, a helix-loop-helix transcription factor, and forced expression of NeuroD1 promotes the differentiation of MB cells. The expression of NeuroD1 in bulk MB cells is repressed by trimethylation of histone 3 lysine-27 (H3K27me3). Inhibition of the histone lysine methyltransferase EZH2 prevents H3K27

*Correspondence: zengjie.yang@fccc.edu.

AUTHOR CONTRIBUTIONS

Conceptualization, Y.C., Y.Z., and Z.-j. Y.; Investigation, Y.C., S.Y.L., G.X., J.H., D.C.G., F.D., A.C., and K.Q.C.; Formal Analysis, S.P., Y.W., D.C.C., A.M.N., D.L.W., A.B., and Z.-j. Y.; Resources, L.Q.C. and R.J.W.; Writing -Original Draft and Review & Editing, Y.C., D.L.W., R.J.W.R., and Z.-j. Y.

SUPPLEMENTAL INFORMATION

Supplemental Information can be found online at https://doi.org/10.1016/j.celrep.2020.107782.

DECLARATION OF INTERESTS

The authors declare no competing interests.

trimethylation, resulting in increased NeuroD1 expression and enhanced differentiation in MB cells, which consequently reduces tumor growth. These studies reveal the mechanisms underlying MB cell differentiation and provide rationales to treat MB (potentially other malignancies) by stimulating tumor cell differentiation.

Graphical Abstract

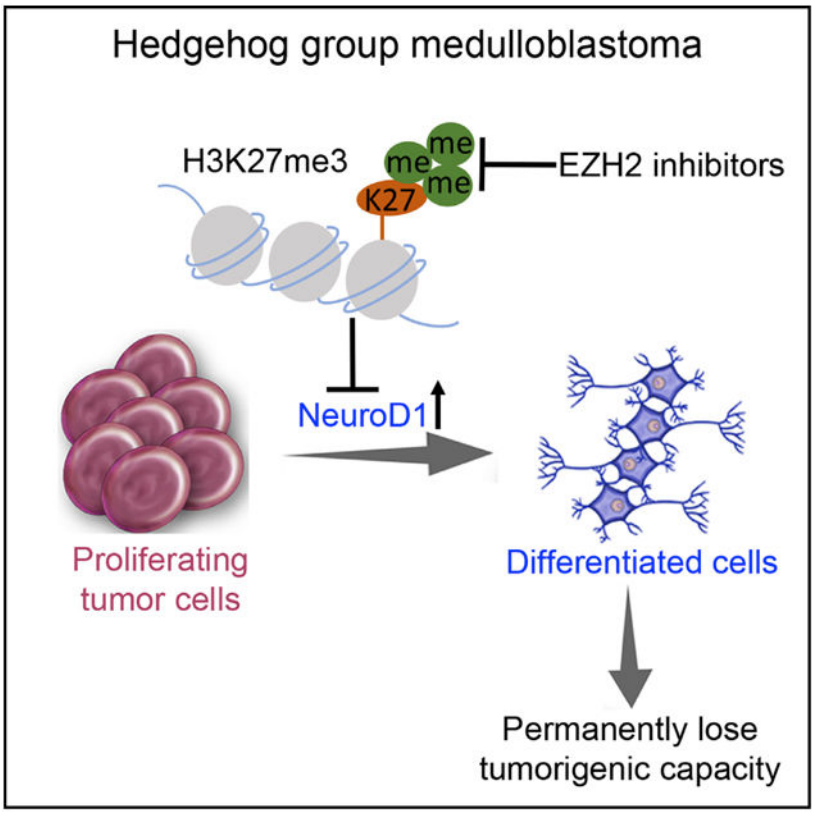

In Brief

Cheng et al. demonstrate that medulloblastoma cells retain the capacity to undergo differentiation. The differentiation of tumor cells is regulated by NeuroD1 expression, which is repressed by H3K27me3 in tumor cells. EZH2 inhibitors suppress medulloblastoma growth by stimulating tumor cell differentiation.

INTRODUCTION

Medulloblastoma (MB) is the most common malignant brain tumor in children. It usually originates from the cerebellum, but it may spread to other parts of the central nervous system (CNS) (Gibson et al., 2010; Romer et al., 2004). Conventional treatment consists of a combined modality approach including surgery, radiation therapy, and chemotherapy, which often cause delayed complications in most patients, such as endocrine disorders and cognitive deficits. Clinical trials and research efforts are now focused on attempts to

decrease treatment toxicity while maintaining a high cure rate in MB patients (Northcott et al., 2019; Packer and Hoffman, 2012).

Human MB consists of at least four subgroups: hedgehog (Hh), Wnt, group 3, and group 4 (Northcott et al., 2012; Taylor et al., 2012). Among these, Hh-MB accounts for at least 30% of human MB. Inactivating mutations in *Patched 1* (*Ptch1*), the antagonizing receptor for Hh ligand, leads to aberrant activation of the Hh pathway, with increased transcription of Hh pathway target genes, including *Ptch2*, *Gli1*, and *Gli2* (Ingham and McMahon, 2001). *Ptch1* heterozygous mice ($Ptch1^{+/-}$) in which one allele of the *Ptch1* gene was replaced with β-galactosidase develop MB in their cerebella at ~30 weeks of age (Goodrich et al., 1997). $Ptch1^{+/-}$ mice are widely used in basic research and preclinical studies of Hh-MB. Group 3 MB represents the most aggressive MB type, exhibiting amplification or overexpression of the MYC oncogene (Cho et al., 2011). Previous studies have demonstrated that cerebellar granule neuron precursors (GNPs) can serve as cells of origin for both Hh-MB and group 3 MB (Kawauchi et al., 2012; Pei et al., 2012; Schüller et al., 2008; Yang et al., 2008).

As the most abundant neuronal progenitors in the brain, GNPs proliferate extensively in the external germinal layer (EGL) at the surface of the cerebellum. After that, GNPs permanently exit the cell cycle and start to differentiate in the deep part of the EGL. As they differentiate, GNPs continue to migrate to their final destination, the internal granule layer (IGL). In the IGL, GNPs become fully differentiated and mature (Goldowitz and Hamre, 1998). The differentiation of GNPs is under a precise spatial/temporal control during cerebellar development.

While the differentiation of neural stem/progenitor cells has been well studied, it still remains unclear whether tumor cells derived from neuronal progenitors can undergo differentiation. By performing single-cell RNA sequencing (scRNA-seq) on a mouse model of MB, we have identified a population of tumor cells that has lost its proliferative capacity and tumorigenic potential and appears to be undergoing differentiation. Resembling GNPs, MB cells extensively express genes associated with neuronal differentiation and maturation as they differentiate. The differentiation of MB cells is regulated by the NeuroD1 expression, and forced expression of NeuroD1 induces differentiation of tumor cells from Hh-MB, indicating that the differentiation overrides oncogenic mutations in MB cells. In the majority of tumor cells, NeuroD1 enhancer and promoter are repressed by trimethylation of histone 3 lysine-27 (H3K27me3). Importantly, pharmacological inhibition of the histone lysine methyltransferase EZH2 prevents H3K27 trimethylation, resulting in increased NeuroD1 expression and enhanced tumor cell differentiation, which consequently reduces tumor growth. These studies demonstrate that MB cells retain the ability to undergo differentiation and pave the way for therapies that target this process.

RESULTS

scRNA-Seq Reveals a Population of Differentiated MB Cells

To examine tumor cell heterogeneity in MB, we performed scRNA-seq on cells dissociated from MB tissue in $Ptch1^{+/-}$ mice. Data from a total of 9,164 cells that met quality control criteria (average 2,130 unique genes per cell) were used for transcriptomic analysis. To

define cell identities and subpopulations, we performed principal-component analysis (PCA) and t-stochastic neighbor embedding (tSNE) analysis. These analyses identified transcriptionally distinct cell clusters corresponding to six broad categories (Figure 1A). Approximately 93% of total analyzed transcriptomes represented tumor cells, distinguished by expression of genes specific for Hh-MB such as *Zic1* and *Barhl1* (Lin et al., 2016; Pöschl et al., 2011; Yokota et al., 2004) (Figure 1B). Based on the expression of well-established markers, we also identified major components of the MB micro-environment, including astrocytes (*Gfap*, *Fabp7*, and *Slc1a3*), oligodendrocytes (*Cspg4*, *Pdgfra*, and *Cntn1*), and microglial cells (*Aif1*, *Cx3cr1*, and *Adgre1*) (Figures 1C and 1D).

Within the tumor cell population, we identified three major clusters of cells: (1) dividing tumor cells that express high levels of genes associated with the cell cycle/division (*Cdk1*, *Ccna2*, and *Cenpf*) and elevated levels of Hh target genes such as *Gli1*, *Gli2*, and *Ptch2*; (2) quiescent tumor cells, in which cell-cycle/division genes have been downregulated but Hh pathway target genes remain activated; and (3) cells expressing low levels of cell-cycle/division genes and low levels of Hh target genes but elevated expression of genes related to neuronal differentiation, including *Cntn2*, *Pax6*, *NeuroD1*, *Tubb3*, and *Gap43* (Figures 1C and 1D). We speculated that the latter population represented tumor cells spontaneously undergoing differentiation. Quiescent, dividing, and differentiated cells accounted for 41%, 30%, and 22% of the total cell population, respectively (Figure 1E). Approximately 7% of the total cell population was composed of stromal cells, including astrocytes, microglia, and oligodendrocytes. Thus, a subset of differentiated cells was found in MB tissue based on scRNA-seq analysis.

t-SNE plots revealed that neuronal differentiation genes, including *Pax6*, *Cntn2*, *NeuroD1*, and *Tubb3*, were enriched in those differentiated MB cells (Figure 1F), whereas the expression of genes associated with cell division, including *Ccna2*, *Ccnb1*, *Cdk1*, and *Cenpf*, was overall downregulated in differentiated tumor cells (Figure 1G). We further analyzed scRNA-seq data obtained from human MB consisting of all four groups (Hh, Wnt, group 3, and group 4) (Hovestadt et al., 2019). Consistent with the previous report (Hovestadt et al., 2019), the four MB groups were well separated based on the genetic profiles of tumor cells (Figure 1H). The distinct population of differentiated tumor cells was readily identified in Hh-group MB based on the elevated expression of neuronal differentiation genes (*Pax6*, *Cntn2*, *NeuroD1*, and *Tubb3*) (Figure 1I). Similar to those differentiated MB cells from *Ptch1*$^{+/-}$ mice, expression levels of cell-cycle genes (*Ccna2*, *Ccnb1*, *Cdk1*, and *Cenpf*) were decreased in differentiated tumor cells in human MB. These data suggest that the differentiation of tumor cells was also present in human MB. All these data confirm that MB cells in both human and mouse can differentiate *in vivo*.

Differentiated MB Cells Are Not Proliferative or Tumorigenic

One gene highly expressed by differentiated tumor cells was *Cntn2* (Figures 1C and 1F), which encodes Tag1, a cell-surface glycoprotein associated with the differentiation and migration of neuronal progenitors (Xenaki et al., 2011). Consistent with our scRNA-seq findings, immunofluorescent staining indicated that a proportion of tumor cells in MB tissue expressed Tag1 (Figures 2A–2C) but were Ki67^{-}, suggesting they were not dividing.

Moreover, Tag1$^+$ cells also expressed MAP2, a marker for neuronal maturation (Fanarraga et al., 1999). These data suggest that Tag1-expressing cells represent differentiated MB cells. To further determine whether Tag1$^+$ cells represent a differentiated subset, we isolated Tag1$^+$ cells from *Ptch1*$^{+/-}$ mice by fluorescence-activated cell sorting (FACS) using an antibody against Tag1. As shown in Figure 2D, ~21% of tumor cells were positive for Tag1. Purified Tag1$^+$ and Tag1$^-$ cells were plated *in vitro*, and pulse-labeled with bromodeoxyuridine (BrdU) for 2 h before being harvested for immunocytochemistry (Figures 2E and 2F). More than 60% of Tag1$^-$ cells were found to be positive for BrdU, whereas less than 10% of Tag1$^+$ cells were BrdU positive (Figure 2G), suggesting that Tag1$^+$ cells were not actively dividing. We next transplanted Tag1$^+$ and Tag1$^-$ cells intracranially into *CB17/SCID* mice to examine the tumorigenicity of these two cell populations (Li et al., 2016; Liu et al., 2017). As shown in Figure 2H, Tag1$^-$ cells gave rise to tumors in *CB17/SCID* mice with 100% penetrance (median survival, 52 days), whereas no tumors arose from Tag1$^+$ cells. The above data suggest that Tag1$^+$ cells have lost proliferative and tumorigenic potential.

Tumors derived from transplantation of Tag1$^-$ cells contained a population of Tag1$^+$ cells comparable to the ~20% of Tag1$^+$ cells found in tumors of *Ptch1*$^{+/-}$ mice, suggesting that proliferating tumor cells can undergo spontaneous differentiation during tumor formation. To further examine this spontaneous differentiation, we lineage traced tumor cells by crossing *Ptch1*$^{+/-}$ mice with *Math1-CreER*^{T2}*/Rosa-GFP* mice in which tumor cells (Math1$^+$) permanently express GFP upon tamoxifen treatment (Yang et al., 2008). At 20 weeks of age, when *Math1-CreER*^{T2}*/Rosa-GFP/Ptch1*$^{+/-}$ mice exhibited signs of intracranial pressure such as ataxia and domed heads, they were treated with tamoxifen by oral gavage. 1 week after tamoxifen treatment, mouse brains were harvested for immunohistochemistry, following intraperitoneal (i.p.) injection of EdU 2 h prior to the sacrifice. As shown in Figure 2I, robust expression of GFP was observed in the cerebellar tumor developed from a *Math1-CreER*^{T2}*/Rosa-GFP/Ptch1*$^{+/-}$ mouse. Differentiated cells (Tag1$^+$) as well as proliferative cells (EdU$^+$) were all found to be positive for GFP (Figures 2J and 2K), indicating that they were all derived from tumor cells. Differentiated cells (Tag1$^+$) and EdU$^+$ cells were mutually exclusive, confirming that differentiated cells were not dividing (Figure 2L).

MB Cells Resemble GNPs in Their Differentiation

Having identified a population of differentiated tumor cells, we next sought to compare tumor cell differentiation with the differentiation of GNPs, the normal cells from which tumors are thought to originate (Schüller et al., 2008; Yang et al., 2008). After proliferating in the superficial EGL (sEGL), GNPs exit the cell cycle and start to differentiate as they migrate into the deep part of the EGL (dEGL). Upon migration to the IGL, GNPs become fully differentiated (Figure 3A). As shown in Figure 3B, Tag1 expression was located in cerebellar dEGL, whereas the sEGL was dominated by dividing GNPs (Ki67$^+$), suggesting that Tag1 expression is initiated as GNPs exit the cell cycle and begin to differentiate in the dEGL. Tag1 expression appears to be lost before GNPs undergo terminal differentiation, since it is absent from mature granule neurons (expressing βIII-tubulin) in the IGL (Figure 3C). The above expression pattern of Tag1 during GNP development was further confirmed by EdU chasing experiments and lineage-tracing assays (Figures S1A–S1H), consistent with previous reports (Furley et al., 1990; Kuhar et al., 1993).

To compare the gene expression profiles of differentiated GNPs and tumor cells, we purified differentiated ($Tag1^+$) and proliferating ($Tag1^-$) GNPs from wild-type cerebella at post-natal day 6 (P6), as well as differentiated ($Tag1^+$) and $Tag1^-$ tumor cells from *Ptch1*$^{+/-}$ mice, and carried out RNA sequencing (RNA-seq) on each population. As revealed by PCA, although proliferating GNPs were well separated from $Tag1^-$ MB cells, differentiated MB cells clustered close to differentiated GNPs, suggesting that differentiation of MB cells resembles that of GNPs (Figure 3D). 1,721 genes differentially expressed between proliferating GNPs and differentiated GNPs, and expression of 1,615 genes was significantly altered between $Tag1^-$ tumor cells and differentiated MB cells (log2 fold change > 1.5 and $p < 0.05$) (Figure 3E). Among these differentially expressed genes, 975 genes were found associated with the differentiation of both GNPs and MB cells. Gene Ontology analysis revealed that these genes were enriched in regulators of the cell cycle and organelle organization (Figure 3F), which is consistent with the cessation of proliferation and process extension during the differentiation of GNPs and MB cells. As shown in Figure 3G, genes associated with neuronal maturation and process extension, including *Mapt*, *L1cam*, and *Stmn2*, were significantly elevated in both differentiated GNPs and MB cells, compared with dividing GNPs and $Tag1^-$ MB cells, respectively. Expression of genes associated with the cell cycle, such as *Cenf* and *Ccna2*, was markedly downregulated in differentiated MB cells and GNPs (Figure 3H). Notably, expression of Hh pathway target genes such as *Gli1* and *Ptch2* was decreased in both differentiated GNPs and MB cells compared with their dividing counterparts (Figure 3I), suggesting that Hh signaling is repressed as both GNPs and MB cells undergo differentiation. Collectively, these data suggest that MB cells differentiate in a similar manner as GNPs.

Differentiation Overrides Hh Pathway Activation

Consistent with our RNA-seq data, qPCR also revealed that expression of *Gli1* and *Gli2* was significantly decreased in differentiated tumor cells ($Tag1^+$) compared with $Tag1^-$ tumor cells ($Tag1^-$) (Figure 4A), further confirming the repression of Hh signaling in differentiated tumor cells. It was previously reported that the remaining wild-type allele of the *Ptch1* gene was lost in MB cells from *Ptch1*$^{+/-}$ mice (Oliver et al., 2005; Tamayo-Orrego et al., 2016). Therefore, we examined the presence of the *Ptch1* gene in the genomic DNAs extracted from GNPs and MB cells by PCR. As expected, compared with wild-type GNPs, GNPs from *Ptch1*$^{+/-}$ mice at P6 yielded approximately half the amount of PCR product of the *Ptch1* gene (Figure 4B). However, almost no PCR product for the *Ptch1* gene was detected in differentiated MB cells ($Tag1^+$) or $Tag1^-$ tumor cells (Figure 4B), suggesting that neither the differentiation capacity nor the reduction in Hh signaling of MB cells resulted from retention of the remaining wild-type allele of *Ptch1*. These findings indicate that Hh signaling was suppressed in differentiated tumor cells despite *Ptch1* deficiency.

To further investigate the effects of differentiation on Hh signaling, we purified $Tag1^-$ tumor cells from *Ptch1*$^{+/-}$ mice by FACS and plated them *in vitro* for 72 h. The majority of freshly isolated $Tag1^-$ cells (0 h) were dividing and exhibited no markers of differentiation (βIII-tubulin) (Figures 4C–4E). However, after 72 h of culture, when almost no proliferation was detected, the MB cells expressed high levels of βIII-tubulin, indicating that they had spontaneously undergo differentiation *in vitro* (Figures 4D and 4E). Expression of *Gli1* and

Gli2 was significantly downregulated in tumor cells as they differentiated *in vitro* (Figure 4F). Infection with a lentivirus carrying *SmoM1* (a constitutively active form of Smo; Murone et al., 1999) or *Gli1* (two effectors downstream of Ptch1 in Hh pathway transduction), effectively activated the Hh pathway in GNPs, as evidenced by significant upregulation of *Ptch2*, a target gene of the Hh pathway (Figure 4G). However, forced expression of *SmoM1* or *Gli1* failed to activate the Hh pathway in MB cells after being cultured for 72 h (Figure 4H), suggesting that the Hh pathway cannot be activated in differentiated tumor cells. Collectively, the above data suggest that differentiation overrides Hh signaling in MB cells.

Enhanced Expression of NeuroD1 Induces MB Cell Differentiation

Our data from scRNA-seq of MB cells revealed that expression of *NeuroD1*, a helix-loop-helix (HLH) transcription factor, was significantly upregulated in differentiated tumor cells compared with other cell populations in MB tissue (Figure 5A). Enhanced expression of *NeuroD1* mRNA and protein was found in differentiated tumor cells ($Tag1^+$) compared with $Tag1^-$ tumor cells purified from mouse MB (Figures 5B and 5C). To examine NeuroD1 expression in tumor tissue and its relationship to proliferation, we performed immunohistochemical staining for NeuroD1 on MB tissue from EdU-pulsed $Ptch1^{+/-}$ mice. Approximately 20% of tumor cells were found to express NeuroD1 protein in mouse MB (Figure 5D). Moreover, the majority of NeuroD1-positive tumor cells were not dividing (negative for EdU) (Figure 5E) but instead co-expressed MAP2, a well-established marker for neuronal differentiation (Figure 5F). These data suggest that MB cells increased NeuroD1 expression as they undergo differentiation. It was previously reported that NeuroD1 expression is required for normal differentiation of GNPs (Miyata et al., 1999; Pan et al., 2009). Elevated expression of NeuroD1 proteins was also observed in differentiated GNPs in the dEGL as well as the IGL compared with dividing GNPs in the sEGL (Figures S1G–S1H). In addition, we examined the association of NeuroD1 expression and tumor cell proliferation in human MB by immunohistochemistry using a tissue microarray (TMA) containing 56 human MB sections. Elevated NeuroD1 expression was inversely associated with proliferation (based on the percentage of $Ki67^+$ cells) in human MB (Figures S2A–S2E) ($p < 0.01$, $r = -0.79$). Collectively, these data suggest that NeuroD1 induction is associated with differentiation of tumor cells in both mouse and human MB.

To examine whether *NeuroD1* can drive tumor cell differentiation, we infected MB cells with a lentivirus encoding *NeuroD1* along with a GFP tag or an empty GFP-encoding vector as a control. MB cells were pulsed with BrdU for 2 h before being harvested for immunocytochemistry. At 48 h post-infection, the majority of tumor cells infected with the control virus were positive for BrdU (Figure 5G), whereas <20% of NeuroD1-infected tumor cells were $BrdU^+$ (Figure 5H). No significant difference in the apoptosis was observed between NeuroD1-infected MB cells and cells infected with the control virus (data not shown). Ectopic expression of NeuroD1 induced tumor cell differentiation, as evidenced by a greater proportion of MB cells expressing MAP2, compared with GFP control (Figures 5I–5K). In addition to MAP2, NeuroD1 also stimulated the expression of other genes associated with neuronal differentiation, including *Mapt*, *L1cam*, and *NeuroD2* (Figure S3A). These data suggest that forced expression of *NeuroD1* repressed tumor cell

proliferation and promoted differentiation. Consistent with our finding that differentiation can override Hh signaling in MB cells, the expression of Hh pathway target genes, including *Gli1* and *Ptch2*, was dramatically repressed in tumor cells after *NeuroD1* overexpression compared with control cells expressing GFP alone (Figure S3B).

Since cell differentiation is always accompanied by the downregulation of Hh signaling in primary MB cells or GNPs, we decided to utilize NIH 3T3 cells to investigate whether *NeuroD1* directly interferes with Hh signaling transduction independent of differentiation induction. For this purpose, we examined Hh signal transduction in NIH 3T3 cells after overexpressing *NeuroD1* or GFP as a control. No alterations in Hh signaling were observed in NIH 3T3 cells after forced expression of *NeuroD1* or GFP (Figures S3C and S3D), indicating that NeuroD1 is insufficient to directly repress Hh signal transduction but is capable of doing so indirectly in MB cells by inducing their differentiation. To examine whether NeuroD1 stimulated differentiation could affect tumorigenesis, we infected MB cells from *Ptch1*$^{+/-}$ mice with a lentivirus encoding NeuroD1-GFP or GFP alone. Infected cells were purified by FACS and transplanted intracranially into *CB17/SCID* mice. As shown in Figure 5L, *NeuroD1* overexpression completely prevented tumor formation in *CB17/SCID* mice (n = 18), while tumor cells infected with the control vector finally developed into tumors with 100% penetrance (n = 16; median survival, 47 days). These data further confirm that NeuroD1-induced differentiation abolishes the tumorigenicity of MB cells.

We further tested the differentiation-promoting effect of *NeuroD1* in human Hh MB cells (ICb-5610MB). Similar to our findings in mouse MB cells, NeuroD1 overexpression significantly decreased the percentage of BrdU^{+} cells and increased the number of βIII-tubulin^{+} cells among MB cells compared with GFP control (Figures 5M–5Q). These data confirm that NeuroD1 can promote the differentiation of both mouse and human MB cells. We next examined the alterations in tumorigenesis of human MB cells after forced expression of *NeuroD1* or GFP as a control by intracranial transplantation. The tumor incidence from NeuroD1-overexpressing MB cells (n = 6) was significantly repressed compared with that from control tumor cells (infected with GFP alone, n = 6; median survival, 34 days) (Figure 5R). These data demonstrate that the tumorigenicity of MB cells was markedly compromised after overexpression of NeuroD1.

NeuroD1 Expression in MB Cells Is Regulated by EZH2-Mediated H3K27me3

Previous studies reported that *NeuroD1* expression in tumor cells, including MB cells, may be regulated by DNA methylation (Fiegl et al., 2008; Hovestadt et al., 2014). However, no difference in methylation of the *NeuroD1* gene was observed between differentiated tumor cells (Tag1^{+}) and Tag1^{-} tumor cells isolated from *Ptch1*$^{+/-}$ MB based on bisulfide sequencing analyses (Figures S4A–S4E). To investigate other possible epigenetic mechanisms regulating NeuroD1 expression in MB cells, we decided to perform a drug-screening assay to identify epigenetic compounds that can regulate NeuroD1 expression in MB cells. MB cells express basal levels of NeuroD1 even before their differentiation; thus, NeuroD1 expression is not a sensitive marker for drug screening. Having observed that increased NeuroD1 expression can repress MB cell proliferation and induce differentiation,

we examined tumor cell proliferation and differentiation after treatment with agents targeting epigenetic regulators.

For this screen, we used a compound library consisting of 244 inhibitors against a variety of epigenetic regulators, including histone deacetylases (HDACs), histone demethylases, and histone acetyltransferases etc. (Figure 6A). $Tag1^-$ tumor cells purified from *Ptch1*$^{+/-}$ mice by FACs were treated with individual compounds at 1 μM for 48 h. Before being collected for immunocyto-chemistry, tumor cells were pulsed with BrdU for 2 h. Compounds were classified as "proliferation repressing" if the percentage of $BrdU^+$ cells in the culture was less than half of that in the control treatment (DMSO) (Figure 6B). Tumor cell differentiation was also examined by immunostaining for p27/Kip1, a nuclear cyclin-dependent kinase inhibitor associated with neuronal differentiation (Nguyen et al., 2006; Sasaki et al., 2000). Compounds were defined as "differentiation promoting" if the percentage of p27/Kip1 was 1.5-fold more than that in the control (Figure 6B). Of the 244 compounds, 51 compounds were found to be proliferation repressing, including 12 compounds that were observed as differentiation promoting. 39 compounds that only inhibited tumor cell proliferation but failed to induce tumor cell differentiation appeared to be cytotoxic. Among the 12 compounds exhibiting the capacity to both repress proliferation and stimulate differentiation of tumor cells were three EZH2 inhibitors (EPZ6438, UNC1999, and GSK126) (Figures 6C–6K). As shown in Figure 6C–6G, treatment with EPZ6438, UNC1999, or GSK126 significantly decreased the percentage of $BrdU^+$ cells among MB cells compared with the vehicle control. Conversely, the percentage of p27/$Kip1^+$ cells in MB cells was enhanced by treatment with EPZ6438, UNC1999, or GSK126 (Figures 6H–6L). Repressed cell proliferation and increased cell differentiation by treatment with EPZ6438, UNC1999, or GSK126 were also observed in human MB cells (Figures S5A–S5J). These data suggest that EZH2 inhibitors can suppress MB cell proliferation and stimulate tumor cell differentiation. We next examined NeuroD1 expression in tumor cells after the treatment with EZH2 inhibitors. As shown in Figure 6M, expression of NeuroD1 protein in tumor cells was dramatically enhanced after treatment with EPZ6438, UNC1999, or GSK126 compared with control treatment. These findings imply that EZH2 may be involved in repressing NeuroD1 expression in MB cells.

To determine the possible role of EZH2 in regulating NeuroD1 expression in MB cells, we examined EZH2 protein in purified differentiated tumor cells ($Tag1^+$) and $Tag1^-$ tumor cells by western blotting. Expression levels of EZH2 protein were significantly elevated in $Tag1^-$ tumor cells compared those in differentiated tumor cells (Figure 6N). EZH2 is a catalytic subunit of the poly-comb repressive complex 2 (PRC2) that is involved in repressing gene expression through trimethylation of histone H3 on lysine 27 (H3K27). Having observed that EZH2 inhibitors increased NeuroD1 expression in MB cells, we next sought to examine whether NeuroD1 expression in MB cells was repressed by EZH2-mediated H3K27me3. Immunohistochemistry revealed that more than 70% of MB cells in *Ptch1*$^{+/-}$ mice were positive for H3K27me3 (Figure 6O). Moreover, majority of NeuroD1-expressing cells were found to be negative for H3K27me3 or EZH2 in MB tissue (Figure 6P and 6Q), consistent with the notion that NeuroD1 expression in MB cells could be silenced by H3K27me3. To test this directly, we performed chromatin immunoprecipitation (ChIP) qPCR analysis for H3K27me3 marked chromatin to determine if the NeuroD1 promoter and enhancer were

modified with H3K27me3 in differentiated and Tag1^{-} tumor cells purified from *Ptch1*$^{+/-}$ MB (Figure 6R) (Amador-Arjona et al., 2015; Feng et al., 2017). H3K27me3 levels at all NeuroD1 promoter and enhancer regions were significantly reduced in differentiated MB cells compared with Tag1^{-} tumor cells (Figure 6S). These data link the changes in NeuroD1 expression that drive MB differentiation to declined EZH2 expression and reduced occupancy of H3K27me3 on the *NeuroD1* loci.

We next infected MB cells with a lentivirus carrying short hairpin RNA (shRNA) specific for EZH2 (#1 and #2) or scrambled shRNA as a control. 48 h following the infection, EZH2 protein levels had declined significantly in tumor cells infected with shRNA specific for *EZH2*, as expected (Figure 6T). The levels of NeuroD1 were elevated in EZH2-deficient tumor cells compared with control tumor cells with scrambled shRNA. EdU incorporation assay revealed that the proliferation was dramatically repressed in MB cells after EZH2 knockdown (Figure 6U). In addition, we overexpressed EZH2 in MB cells by infection with a lentivirus encoding EZH2 or GFP alone as a control. The enhanced levels of EZH2 protein were confirmed in MB cells after forced expression of EZH2 (Figure 6V). NeuroD1 expression was obviously repressed in MB cells with EZH2 overexpression compared to the control tumor cells with GFP alone (Figure 6V). The proliferation of MB cells was increased after forced expression of EZH2, based on the EdU incorporation assay (Figure 6W). These data further demonstrate that NeuroD1 expression was suppressed in MB cells by EZH2-mediated H3K27me3.

Histone acetylation is often associated with transcriptional activation (Creyghton et al., 2010; Ernst et al., 2011). Interestingly, ChIP qPCR revealed increased occupancy of H3K27ac on loci of NeuroD1 promoter and enhancer regions in differentiated MB cells (Figure S6A). Consistent with this, elevated levels of H3K27ac were observed in differentiated MB cells, which were correlated with increased expression of NeuroD1 (Figure S6B). These data imply that H3K27ac may be involved in the induction of NeuroD1 expression during MB cell differentiation.

EZH2 Inhibitors Repress MB Growth by Promoting Tumor Cell Differentiation

Having observed that tumor cell differentiation was driven by NeuroD1 and that NeuroD1 expression in MB cells is repressed by EZH2, we next examined the efficacy of EZH2 inhibitors (UNC1999, EPZ6438, and GSK126) for MB treatment.

MB cells isolated from *Ptch1*$^{+/-}$ mice were treated with UNC1999, EPZ6438, or GSK126 at various concentrations for 48 h. As shown in Figures 7A–7C, all three compounds repressed cell proliferation in a dose-dependent manner. The IC_{50}s (concentrations required to inhibit tumor cell viability by 50%) of UNC1999, GSK126, and EPZ6438 in repressing proliferation of *Ptch1*-deficient MB cells were 2.08 μM, 4.64 μM, and 8.74 μM, respectively.

To test whether inhibition of EZH2 can repress the proliferation of drug-resistant MB cells, we infected cerebellar GNPs with a lentivirus encoding SmoA1 (W539L), a constitutively activated form of Smo that renders the resistance of MB cells to vismodegib, an FDA-approved inhibitor of Hh pathway (Rudin et al., 2009; Xie et al., 1998; Yauch et al., 2009). 48 h following the infection, cells were treated with vismodegib, EZH2 inhibitors, or DMSO

as a control. As expected, vismodegib failed to inhibit the proliferation of SmoA1-expressing GNPs (Figures 7D and 7E). However, UNC1999, GSK126, or EPZ6438 significantly repressed the proliferation of SmoA1-expressing cells. These data suggest that EZH2 inhibitors can suppress the proliferation of drug-resistant MB cells.

It was previously reported that EZH2 inhibitors, including UNC1999, GSK126, and EPZ6438, could not efficiently penetrate the blood-brain barrier (Zhang et al., 2015). Therefore, to test the effects of these compounds on tumor growth *in vivo*, we then generated subcutaneous MB models by injecting tumor cells from *Ptch1*$^{+/-}$ mice into the flank of *CB17/SCID* mice (Gordon et al., 2018; Kim et al., 2010). After tumors were established, tumor-bearing mice were treated with UNC1999 or GSK126 at dosages of 50 mg/kg and 100 mg/kg or vehicle control (methylcellulose) once a day by oral gavage. As shown in Figure 7F, steady tumor growth was observed in the control group, with tumor volume reaching 2,000 mm^3 by 10 days after the treatment. Compared with the control, GSK126 and UNC1999 significantly repressed tumor growth (Figure 7G). Both drugs exhibited obvious dose-dependent efficacies in reducing MB growth, indicating that EZH2 inhibitors can suppress the growth of MB cells *in vivo*. To further investigate the basis for EZH2-inhibitor-repressed MB growth, subcutaneous tumors after drug treatment were harvested for immunohistochemistry. No significant weight loss was observed in mice treated with EZH2 inhibitors compared with control (data not shown). As shown in Figures 7G and 7H, the majority of tumor cells in the control group were proliferative (Ki67$^+$), whereas proliferation of tumor cells was significantly decreased after treatment with either UNC1999 or GSK126. A marked increase in differentiation (NeuN expression) was also observed in tumor tissue after treatment with EZH2 inhibitors, compared with only a few NeuN$^+$ cells present in control tumors (Figures 7G and 7I). In addition, enhanced apoptosis was found in tumor tissue upon the treatment with EZH2 inhibitors (Figures 7G and 7J). Treatment with UNC1999 or GSK126 significantly induced NeuroD1 expression in tumor tissues compared with the control (Figure 7K). These data suggest that EZH2 inhibitors effectively suppress MB growth by promoting tumor cell differentiation and repressing tumor cell proliferation.

To test the effects of EZH2 inhibitor on the growth of endogenous MB, we treated MB from *Ptch1*$^{+/-}$ mice with EPZ6438. To facilitate blood-brain barrier penetration of EPZ6438, we pre-treated tumor-bearing mice with elacridar at 4 h prior to oral treatment with EPZ6438 or vehicle control (Figure S7A), as previously described (Jin et al., 2017). After treatment for 15 days, MB tissues were collected to examine tumor cell proliferation and differentiation by immunohistochemistry. Compared with the control, EPZ6438 treatment significantly repressed tumor cell proliferation (Figures S7B and S7C) and dramatically induced tumor cell differentiation (Figures S7B–S7D). NeuroD1 expression was markedly elevated in tumor tissues following the treatment with EPZ6438 (Figure S7E). These data further confirm that inhibition of EZH2 enhanced NeuroD1 expression in MB cells and promoted tumor cell differentiation. Finally, a MB mouse model was generated by intracranially injection of human Hh MB cells into *CB17/SCID* mice (ICb-5610MB). After MB was established, tumor-bearing mice were treated with EPZ6438 or vehicle control as described above. After treatment for 15 days, EPZ6438 markedly inhibited tumor cell proliferation

(Figures S7F and S7G) and stimulated MB differentiation (Figures S7F–S7H). These data confirm the efficacy of EZH2 inhibitors in suppressing the growth of Hh-group MB.

DISCUSSION

It is widely accepted that tumor cells are characterized with unlimited replication as well as perturbed differentiation. These features of tumor cells stand in marked contrast to normal stem/progenitor cells, which can only divide a limited number of times before undergoing differentiation (Hanahan and Weinberg, 2011). Here, we demonstrate that MB cells maintain the capacity to differentiate in a manner similar to GNPs, the cells from which they originate. A rare population of cancer stem cells ($Sox2^{+}$) was previously found to differentiate into mature granule neurons in MB tissue (Vanner et al., 2014). Differentiated tumor cells irreversibly exit the cell cycle, lose their tumorigenic potential, and express genes associated with neuronal differentiation and maturation. In our studies, tumor cells proceed to differentiate despite oncogenic mutations such as *Ptch1* deficiency. These findings are consistent with the hypothesis of Pierce and colleagues that cell differentiation can override oncogenic mutations/transformation (Pierce, 1983; Pierce and Wallace, 1971). During normal development, the Hh pathway is activated in GNPs in response to Shh secreted by Purkinje neurons (Dahmane and Ruiz i Altaba, 1999; Wechsler-Reya and Scott, 1999). However, Hh signaling is repressed in GNPs when they initiate differentiation. Since GNPs migrate toward Purkinje neurons as they start to differentiate, it still remains unclear how Hh signaling is inactivated in GNPs in such a Shh-rich environment. Our finding that differentiation can override Hh signaling in MB cells suggests that differentiation intrinsically suppresses Hh signaling in GNPs.

Numerous studies have reported that MB cells resemble cerebellar GNPs in their morphology and expression of characteristic markers (Pomeroy et al., 1997; Salsano et al., 2004; Yokota et al., 1996). Several recent studies elegantly demonstrated that human MB derives from disturbed development of cerebellum by single-cell transcriptomics (Hovestadt et al., 2019; Vladoiu et al., 2019). Here, we further reveal that MB cells resemble GNPs in their capacity for differentiation. These results implicate that tumor cells can be “normalized” into nonmalignant cells. Our findings are consistent with previous discoveries of Mintz and colleagues, who reported that after being injected into very early mouse embryos, teratoma cells participated in the normal development of the recipient mouse instead of forming malignancies (Mintz and Illmensee, 1975). The normalization capacity of tumor cells argues that oncogenic transformation is a reversible process. In our studies, the bulk population of MB cells ($Tag1^{-}$) consists of proliferating tumor cells, and a significant proportion of cells appear to be quiescent based on the scRNA-seq data. Future studies are warranted to further investigate the role of those quiescent cells in the initiation and progression of MB.

NeuroD1, a type E HLH transcription factor, was previously found to be necessary for differentiation of normal GNPs (Gao et al., 2009; Miyata et al., 1999). Deletion of NeuroD1 disrupted GNP differentiation by prolonging the proliferation and induction of apoptosis in developing cerebella (Miyata et al., 1999; Pan et al., 2009). Here, we found that NeuroD1 mRNA expression was markedly increased in differentiated tumor cells compared with bulk

tumor cells in MB and forced expression of NeuroD1 promoted tumor cells differentiation. These data demonstrate that NeuroD1 drives tumor cell differentiation in MB. Basal levels of NeuroD1 expression were not absent in bulk tumor cells in MB. Knockdown of NeuroD1 expression in MB cells by shRNA caused extensive cell death (data not shown), in agreement with neuronal death observed in NeuroD1-null mice (Gao et al., 2009). It was recently reported that NeuroD1 acts as a key transcriptional mediator for group 3 MB (Boulay et al., 2017). These findings indicate that NeuroD1 may have other functions besides differentiation induction during MB initiation and progression.

A previous study reported that bone morphogenic proteins (BMPs) can induce the differentiation of both GNPs and MB cells through post-transcriptional downregulation of Atoh1(Zhao et al., 2008). Consistent with our studies, MB growth was inhibited following the differentiation of tumor cells after BMP treatment. However, the levels of NeuroD1 as well as Zic1 and Pax6 proteins were either unchanged or even slightly decreased in GNPs *in vitro* upon BMP treatment, although these proteins are well-established markers for normal differentiation of GNPs (Lewis et al., 2004). Future studies are warranted to examine whether similar changes in the protein levels of Zic1, Pax6, and NeuroD1 can be found in MB cells after BMP treatment.

It was previously reported that NeuroD1 expression in many malignancies, such as breast cancer and MB, can be regulated by DNA methylation (Fiegl et al., 2008; Hovestadt et al., 2014). However, no difference in DNA methylation of NeuroD1 gene was observed between differentiated tumor cells and bulk tumor cells in MB cells from $Ptch1^{+/-}$ mice. These data indicate that upregulation of NeuroD1 expression in differentiated MB cells may not be due to DNA methylation. By screening epigenetic compounds, we found that EZH2 inhibitors induced MB cell differentiation and enhanced NeuroD1 expression in MB cells. The expression of EZH2 mRNA and protein was significantly declined in differentiated MB cells. These data, together with our ChIP-PCR analysis, demonstrate that NeuroD1 expression in bulk tumor cells is repressed by EZH2-mediated H3K27me3. The increased occupancy of H3K27ac on NeuroD1 enhancer loci in differentiated MB cells suggests that NeuroD1 expression may be induced by H3K27ac during MB differentiation. Indeed, forced expression of EZH2 inhibited NeuroD1 expression in MB cells, whereas NeuroD1 expression was upregulated in MB cells following the EZH2 knockdown. These findings shed light on the molecular basis of NeuroD1 expression in MB cells, highlighting the important role of epigenetic regulations during MB progression.

In our studies, EZH2 inhibitors upregulated NeuroD1 expression in Hh-MB cells, and repressed the *in vivo* growth of Hh-MB. Interestingly, it was recently reported that *EZH2* inactivation promoted the progression of group 3 MB by upregulation of *Gfi1* (Vo et al., 2017). These findings suggest that EZH2 may exert distinct functions in different MB subgroups.

Traditional radiotherapy and chemotherapy act by damaging or killing tumor cells. However, these therapies often cause side effects that severely affect quality of life. Almost all MB patients suffer long-term adverse effects from these cytotoxic drugs, such as cognitive deficits and endocrine disorders (Taylor et al., 2012; Ullrich and Pomeroy, 2003).

Differentiation therapy represents a more targeted and less toxic approach to tumor treatment (de Thé, 2018; Enane et al., 2018; Gailhouste et al., 2018; Manegold et al., 2018). The underlying premise of differentiation therapy is that tumor cells can be reprogrammed to differentiate, thereby inhibiting tumor progression (Leszczyniecka et al., 2001). As a standard therapeutic strategy for acute promyelocytic leukemia, all-trans-retinoic acid induces the cancer cells to differentiate from a granulocyte precursor into a mature myelocyte that can no longer divide (Cicconi and Lo-Coco, 2016; Wang and Chen, 2008). Here, we demonstrate that EZH2 inhibitors can induce NeuroD1 expression in *Ptch1*-deficient MB cells and promote their differentiation, thereby inhibiting tumor cell proliferation. More importantly, EZH2 inhibitors, including UNC1999, GSK126, and EPZ6438, significantly suppress the proliferation of SmoA1-expressing GNPs that are resistant to vismodegib, indicating that inhibition of EZH2 could be applied to treat drug-resistant MB cells. In our studies, EZH2 inhibitors exhibited promising efficiency in inducing tumor cell differentiation and suppressing the growth of human and mouse MB cells *in vivo*. Elevated levels of apoptosis were observed in MB tissues following treatment with EZH2 inhibitors, which are likely due to the ectopic differentiation among tumor cells *in vivo* as reported previously (Vanner et al., 2014). EZH2 inhibitors induced significant differentiation in tumor cells *in vitro*, without inducing apoptosis. These data suggest that the repressed tumor growth after EZH2 treatment was predominately due to the enhanced differentiation of MB cells resulting from the upregulation of NeuroD1. As a repressive histone modification, H3K27me3 has been implicated in regulating the expression of many genes. It remains possible that other target genes of H3K27me3 are involved in the tumor-suppressing effects of EZH2 inhibitors.

Our studies provide rationales for utilizing EZH2 inhibitors in MB treatment. Clinical trials with EZH2 inhibitors are currently ongoing across a wide spectrum of malignancies, including pediatric lymphoma, prostate cancer, and solid tumors, and many have obtained a promising response in patients (Fioravanti et al., 2018). To treating MB by targeting EZH2, future studies are needed to develop brain-penetrant EZH2 inhibitors or strategies to deliver these drugs to the CNS.

STAR★METHODS

RESOURCE AVAILABILITY

Lead Contact—Further information and requests for resources and reagents should be directed to and will be fulfilled by the Lead Contact, Zeng-jie Yang (Zengjie.Yang@fccc.edu).

Materials Availability—No reagents were generated in this study.

Data and Code Availability—The single-cell RNA sequencing data generated in this study are available at NCBI Gene Expression Omnibus (accession number: GSE150752). The code used is available on request.

EXPERIMENTAL MODEL AND SUBJECT DETAILS

Mice—*Ptch1*+/− mice, *Math1-Cre*ER^{T2} mice, *Math1-Cre* mice and *Rosa-GFP* mice were purchased from the Jackson Laboratory. *CB17/SCID* mice were bred in the Fox Chase Cancer Center Laboratory Animal Facility (LAF). All animals were maintained in the LAF at Fox Chase Cancer Center and all experiments were performed in accordance with procedures approved by the Fox Chase Cancer Center Animal Care and Use Committee. All mice were bred and genotyped as recommended by the Jackson Laboratory. For all mouse studies, mice of either sex were used. Ages of all mice used in experiments are indicated in the figure legends.

METHOD DETAILS

Cell culture and CCK8 assay—For examining the *in vivo* efficacies, the stock solutions of UNC1999, GSK126 and EPZ6438 (in DMSO, 100mg/ml) were diluted using 0.5% methylcellulose plus 0.2% Tween-80 (MCT), which were administrated to mice by oral gavage. To facilitate the brain penetration of EPZ6438, Elacridar (100mg/kg) dissolved in DMSO/corn oil (1:9), was orally gavaged 4 hr prior to EPZ6438 treatment. Tamoxifen (Sigma-Aldrich, T5648) was dissolved at a concentration of 20 mg/ml in corn oil and administrated once by oral gavage at a dosage of 200 mg/kg. MB tissues were harvested at 1 week following the tamoxifen treatment.

GNPs and MB cells were isolated from wild-type mice at P7, and *Ptch1*+/− mice at 30 weeks of age, respectively. Cerebella or tumor tissue were digested in a papain solution to obtain a single-cell suspension and then centrifuged through a 35% and 65% Percoll gradient. Cells from the 35% to 65% interface were suspended in Dulbecco's PBS (DPBS) plus 0.5% BSA. Cells were then suspended in NB-B27 (Neurobasal with 1 mM sodium pyruvate, 2 mM L-glutamine, B27 supplement and 1% Pen/Strep, all from Invitrogen) and plated on poly-D-lysine (PDL)-coated coverslips (BD Biosciences). NIH 3T3 cells were cultured in DMEM with 10% fetal bovine serum, 1% Pen/Strep and 2mM L-glutamine (Invitrogen).

The cell survival was determined using Cell Counting Kit-8 (CCK-8) kit. MB cells were plated at a density of 2×10^5 cells/well in 96-well multiplates. After drug treatment for 48 hr, 10 μL of CCK-8 solution was added to each well and further incubated for 2 hr. Then, the absorbance values were detected at a wavelength of 450 nm using a Bio-Rad microplate reader. The cell viability was calculated by the optical density (OD) values of treated groups/OD values of control groups × 100%. In some experiments, cells were pulsed with BrdU (10μM) for 2 hr before being harvested to examine cell proliferation by immunocytochemistry.

Tumor transplantation—MB cells were injected into the cerebella of *CB17/SCID* mice using a stereotaxic frame with a mouse adaptor (David Kopf Instruments), as described previously (Yang et al., 2008). Before transplantation, MB cells were infected with lentivirus carrying GFP-tagged NeuroD1 or empty GFP vector for 24hrs, and infected MB cells (GFP +) were then purified by FACS. For transplantation with MB cells (human or mouse) after the virus infection, the cell suspension was centrifuged at 900rpm for 5 mins to remove the

supernatant (containing dead cells). 5×10^5 viable cells (based on Trypan blue staining) were injected into the cerebellum of each mouse. Survival was defined as the time from transplantation until symptom onset.

CB17/SCID male mice of age 6–8 weeks were used for subcutaneous allograft establishment. Cells isolated from tumor-bearing mice in a single-cell suspension in PBS at concentration 2×10^6 cells was mixed with reduced growth factor Matrigel (Corning) in a 20:80 ratio and injected subcutaneously on the flank of *CB17/SCID* mice. 4 weeks following injection, tumor-bearing mice that satisfied initial tumor volume requirement (200–400mm^3) were randomized into experimental groups. Compounds were administrated once a day and tumor size measurements were taken every day and tumor volume calculated as described previously (Tomayko and Reynolds, 1989).

Immunostaining, flow cytometry, western blotting and TMA analysis— Immunofluorescent staining of sections and cells was carried out according to standard methods. Briefly, sections or cells were blocked and permeabilized for 1 hr with PBS containing 0.1% Triton X-100 and 10% normal goat serum, stained with primary antibodies overnight at 4°C, and incubated with secondary antibodies for 2 hr at room temperature. Sections or cells were counter-stained with DAPI and mounted with Fluoromount-G (Southern Biotech) before being visualized using a Nikon Eclipse Ti microscope. For purifying differentiated MB cells, tumor cells were incubated with the primary antibody against Tag1 (1:50, mouse IgM, DSHB) on ice for 30 mins. After washing with PBS for 3 times, tumor cells were incubated with Texas Red-conjugated secondary antibody for 30 mins. Tag1- tumor cells and differentiated tumor cells (Tag1+) were then fractionated by FACs. In some experiments, MB-bearing mice were treated with EdU (10mg/ml) by intraperitoneal injection, at 2hrs before sacrifice.

For western blot analysis, cells were lysed in RIPA buffer (Thermo) supplemented with protease and phosphatase inhibitors (Thermo). Total lysate containing equal amount of protein were separated by SDS-PAGE gel and subsequently transferred onto PVDF membrane. Membranes were then subjected to probe with antibodies. Western blot signals were detected by using Super-Signal West Pico Chemiluminescent substrate (Thermo) and exposed on films.

Totally human MB TMAs containing a total of 126 (duplicate) cores from 63 samples (including 56 MB samples and 7 control tissue samples) were used for analyzing the correlation between NeuroD1 expression and tumor cell proliferation. After immunostaining with antibodies against Ki67 or NeuroD1, the slides were independently viewed and scored by two experienced pathologists. H-score was generated for NeuroD1 expression on the slide. The H score consists of the product of the intensity of nuclearstaining (0–3+) and the percentage of cells with nuclear staining. The range of the H score was 0 to 300 (0% cells positive to 100% cells 3+positive). The correlation between H score of NeuroD1 expression and the percentage of Ki67+ cells, was analyzed by calculating the spearman rho correlation coefficient.

Q-PCR, DNA methylation assay and ChIP-PCR—RNA was isolated using the RNAqueous kit (Ambion) and treated with DNA-free DNase (Ambion). cDNA was synthesized using oligo(dT) and Superscript II reverse transcriptase (Invitrogen). Quantitative PCR reactions were performed in triplicate using iQ SYBR Green Supermix (Bio-Rad) and the Bio-Rad iQ5 Multicolor Real-Time PCR Detection System. Primer sequences are available upon request.

For DNA methylation assay, genomic DNA was subjected to the sodium bisulfite modification reaction as previously described. Products from the bisulfite reactions were amplified by PCR using primers designed with the MethPrimer software at http://www.urogene.org/methprimer/. Purified PCR products were subcloned into pGEM T-Easy vector (Invitrogen), and individual inserts from 10–15 clones were sequenced.

For ChIP-PCR, MB cells were fixed with 1% formaldehyde for 10minutes at room temperature, and then quenched by incubation with glycine for 10 minutes. Cells were lysed with 1 mL Lysis Buffer 1 (50mM HEPES-KOH, 140 mM NaCl, 1mM EDTA, 10% glyerol, 0.5% NP-40, 0.25% Triton X-100) at 4°C for 10 minutes. After spinning for 5 min at 700xg at 4°C, cells were washed with 1 mL Lysis Buffer 2 (10mM Tris-HCl, 200mM NaCl, 1mM EDTA, 0.5mM EGTA) at 4°C for 10 minutes. The nuclei were pipetted in 200 μL Lysis Buffer 3 (50mM Tris-HCl, 1%SDS, 10mM EDTA). After sonication, the cell lysate was centrifuged to collect the supernatant. Protein G Dynabeads (Life technologies) were used to binding antibody against H3K27me3 or H3K27ac, and immuno-precipitated with diluted chromatin at 4°C on rotating overnight. Rabbit IgG as a negative control. The chromatin/antibody-beads mixture was washed and eluted with 200ul Elution Buffer (10mM Tris-HCl, 0.5% SDS, 300mM NaCl, 5mM EDTA) to reverse crosslinks at 65°C overnight. The DNA were purified and extracted by ChIP DNA Clean and Concentrator Kit (Zymo) according to the manufacturer's protocol. ChIP-PCR was performed using the purified DNA as a template (ChIP 1:2, input 1:10), and quantified by SYBR Green PCR Kits (QIAGEN). To compare the enrichment of DNA pulled down by H3K27me3 or H3K27ac antibody at potential binding sites between Tag1+ and Tag1- populations, ChIP-qPCR data were normalized and relative to 2% of input DNA.

Single-Cell RNA Sequencing and data analyses—Viable single cells were loaded on to a 10X Genomics Chromium Controller instrument to generate single-cell barcoded droplets (GEMs) using the 10x Single Cell 3′ Gel Bead Kit and 10x Chromium system at GENEWIZ following as the manufacturer's protocol. Briefly, single cells were partitioned into Gel Beads in Emulsion (GEMs) in the Chromium Controller instrument with cell lysis and barcoded reverse transcription of RNA, followed by cDNA amplification, shearing, library construction and indexing by PCR amplification. Subsequently, libraries were sequenced by Illumina 2×150 bp sequencing.

The Cell Ranger Single Cell Software Suite v.2.0.1 (https://support.10xgenomics.com/) by 10x Genomics was used to perform sample de-multiplexing, barcode processing and single-cell 3′ gene counting. In brief, base call files were fastq format were aligned to the mm10 reference genome that used an aligner called STAR with default settings, and aligned reads were filtered for valid cell barcodes and UMI to generate filtered gene-barcode matrices. The

pre-processed 10X and DGE matrices were then imported using the Seurat package for the R programming language (version 3.5.4), and the data were filtered to include genes detected in > 5 cells, and cells with 500~6000 detected genes and UMI with 1000~30000 and < 15% mitochondrial genes. For single-dataset analyses, Log-normalized expression values were obtained by the NormalizeData function, and variable genes were identified using the FindVariableGenes Seurat function, TPM values were obtained from raw UMI counts by normalizing with total UMI counts per cell. Next, Principle components analysis (PCA) was performed and significant PCs were used as input for graph-based clustering. 2-dimensional visualization of the multi-dimensional dataset was done with t-SNE. For clustering, we used the function FindClusters that implements SNN (shared nearest neighbor) modularity optimization based clustering algorithm on 15 PCA components with resolution 0.1–0.5, leading to 5–12 clusters. A resolution of 0.25 was chosen for the analysis.

Single cell gene expression profiling data from human MB (GSE119926) were obtained from the Gene Expression Omnibus (GEO) database (https://www.ncbi.nlm.nih.gov/geo/). After pretreatment of raw data and preparation of profile matrix, Seurat3 R package was used for further data analysis.

Profiling differentially expressed genes within each cell cluster—To identify differentially expressed genes in each cell cluster, we applied the FindAllMarkers function from Seurat to the normalized gene expression data. Here, we selected a power value greater than 0.25 as the cut-off for gene selection. The gene expression levels plotted by packages in R. For cell type analysis, we performed differentially expressed gene (DEG) analysis by comparing each cluster with the other clusters using the Wilcoxon rank sum test. Genes with scaled dispersion > 0.25 and log-normalized average expression > 0.01 were included in the analyses. For each cluster, DEGs with top 1.5 fold changes were designated as a cell type signature, Thresholds were set as P value < 0.05. If a cell type signature gene overlapped among different clusters, the gene was assigned to the cluster having the highest expression value. To characterize clusters, we used known marker genes that was reported to compare the differentially expressed gene use GeneQuery and Enrichment analysis. For heatmap representation, normalized expression of markers inside each cluster was used.

RNA sequencing—Total RNA was extracted from purified GNPs and MB cells. Strand-specific mRNA-seq libraries for the Illumina platform were generated and sequenced at at GENEWIZ following the manufacturer's protocol. High-quality total RNA was used as input for the so-called dUTP library preparation method. Briefly, the mRNA fraction was purified from total RNA by polyA capture, fragmented and subjected to first-strand cDNA synthesis with random hexamers in the presence of Actinomycin D. The second-strand synthesis was performed incorporating dUTP instead of dTTP. Barcoded DNA adapters were ligated to both ends of the double-stranded cDNA and subjected to PCR amplification. The resultant library was checked on a Bioanalyzer (Agilent) and quantified. The libraries were multiplexed, clustered, and sequenced on an Illumina HiSeq 2000. The sequencing run was analyzed with the Illumina CASAVA pipeline (v1.8.2), with demultiplexing based on sample- specific barcodes. The raw sequencing data produced was processed removing the

sequence reads which were of too low quality (only “passing filter” reads were selected) and discarding reads containing adaptor sequences or PhiX control with an in-house filtering protocol.

QUANTIFICATION AND STATISTICAL ANALYSIS

Student’s t test was performed to determine the statistical significance of the difference. $p < 0.05$ was considered statistically significant (*, $p < 0.05$; **, $p < 0.01$; ***, $p < 0.001$; ****, $p < 0.0001$; ns, not significant). Error bars represent the SEM. Overall survival was assessed using the Kaplan-Meier survival analysis and the Mantel-Cox log-rank test was used to assess the significance of difference between survival curves. Data handling and statistical processing was performed using Microsoft Excel and Graphpad Prism Software.

Supplementary Material

Refer to Web version on PubMed Central for supplementary material.

ACKNOWLEDGMENTS

We would like to thank Drs. Andrey Efimov, Joe Hurley, and James Oesterling for technical assistance; Dr. Xiaonan Li for providing human MB PDX lines; and Drs. Mariarita Vicini and Daniel Martinez for human MB TMA analysis. This research was supported by the NCI (grant CA178380 to Z.-j. Y.), the ACS RSG (grant RSG1605301NEC to Z.-j. Y.), American Brain Tumor Association (grant DG1900025 to Z.-j. Y.) and the PA CURE Health Research Fund (grant CURE 4100068716 to Z.-j. Y.).

REFERENCES

Amador-Arjona A, Cimadamore F, Huang CT, Wright R, Lewis S, Gage FH, and Terskikh AV (2015). SOX2 primes the epigenetic landscape in neural precursors enabling proper gene activation during hippocampal neurogenesis. Proc. Natl. Acad. Sci. USA 112, E1936–E1945. [PubMed: 25825708]

Boulay G, Awad ME, Riggi N, Archer TC, Iyer S, Boonseng WE, Rossetti NE, Naigles B, Rengarajan S, Volorio A, et al. (2017). OTX2 activity at distal regulatory elements shapes the chromatin landscape of group 3 medulloblastoma. Cancer Discov. 7, 288–301. [PubMed: 28213356]

Cho YJ, Tsherniak A, Tamayo P, Santagata S, Ligon A, Greulich H, Berhoukim R, Amani V, Goumnerova L, Eberhart CG, et al. (2011). Integrative genomic analysis of medulloblastoma identifies a molecular subgroup that drives poor clinical outcome. J. Clin. Oncol 29, 1424–1430. [PubMed: 21098324]

Cicconi L, and Lo-Coco F (2016). Current management of newly diagnosed acute promyelocytic leukemia. Ann. Oncol 27, 1474–1481. [PubMed: 27084953]

Creyghton MP, Cheng AW, Welstead GG, Kooistra T, Carey BW, Steine EJ, Hanna J, Lodato MA, Frampton GM, Sharp PA, et al. (2010). Histone H3K27ac separates active from poised enhancers and predicts developmental state. Proc. Natl. Acad. Sci. USA 107, 21931–21936. [PubMed: 21106759]

Dahmane N, and Ruiz i Altaba A (1999). Sonic hedgehog regulates the growth and patterning of the cerebellum. Development 126, 3089–3100. [PubMed: 10375501]

de Thé H (2018). Differentiation therapy revisited. Nat. Rev. Cancer 18, 117–127. [PubMed: 29192213]

Enane FO, Saunthararajah Y, and Korc M (2018). Differentiation therapy and the mechanisms that terminate cancer cell proliferation without harming normal cells. Cell Death Dis. 9, 912. [PubMed: 30190481]

Ernst J, Kheradpour P, Mikkelsen TS, Shoresh N, Ward LD, Epstein CB, Zhang X, Wang L, Issner R, Coyne M, et al. (2011). Mapping and analysis of chromatin state dynamics in nine human cell types. Nature 473, 43–49. [PubMed: 21441907]

Fanarraga ML, Avila J, and Zabala JC (1999). Expression of unphosphorylated class III beta-tubulin isotype in neuroepithelial cells demonstrates neuroblast commitment and differentiation. Eur. J. Neurosci 11, 517–527. [PubMed: 10073918]

Feng W, Kawauchi D, Körkel-Qu H, Deng H, Serger E, Sieber L, Lieberman JA, Jimeno-González S, Lambo S, Hanna BS, et al. (2017). Chd7 is indispensable for mammalian brain development through activation of a neuronal differentiation programme. Nat. Commun 8, 14758. [PubMed: 28317875]

Fiegl H, Jones A, Hauser-Kronberger C, Hutarew G, Reitsamer R, Jones RL, Dowsett M, Mueller-Holzner E, Windbichler G, Daxenbichler G, et al. (2008). Methylated NEUROD1 promoter is a marker for chemosensitivity in breast cancer. Clin. Cancer Res 14, 3494–3502. [PubMed: 18519782]

Fioravanti R, Stazi G, Zwergel C, Valente S, and Mai A (2018). Six years (2012–2018) of researches on catalytic EZH2 inhibitors: the boom of the 2-pyridone compounds. Chem. Rec 18, 1818–1832. [PubMed: 30338896]

Furley AJ, Morton SB, Manalo D, Karagogeos D, Dodd J, and Jessell TM (1990). The axonal glycoprotein TAG-1 is an immunoglobulin superfamily member with neurite outgrowth-promoting activity. Cell 61, 157–170. [PubMed: 2317872]

Gailhouste L, Liew LC, Yasukawa K, Hatada I, Tanaka Y, Nakagama H, and Ochiya T (2018). Differentiation therapy by epigenetic reconditioning exerts antitumor effects on liver cancer cells. Mol. Ther 26, 1840–1854. [PubMed: 29759938]

Gao Z, Ure K, Ables JL, Lagace DC, Nave KA, Goebbels S, Eisch AJ, and Hsieh J (2009). Neurod1 is essential for the survival and maturation of adult-born neurons. Nat. Neurosci 12, 1090–1092. [PubMed: 19701197]

Gibson P, Tong Y, Robinson G, Thompson MC, Currle DS, Eden C, Kranenburg TA, Hogg T, Poppleton H, Martin J, et al. (2010). Subtypes of medulloblastoma have distinct developmental origins. Nature 468, 1095–1099. [PubMed: 21150899]

Goldowitz D, and Hamre K (1998). The cells and molecules that make a cerebellum. Trends Neurosci. 21, 375–382. [PubMed: 9735945]

Goodrich LV, Milenković L, Higgins KM, and Scott MP (1997). Altered neural cell fates and medulloblastoma in mouse patched mutants. Science 277, 1109–1113. [PubMed: 9262482]

Gordon RE, Zhang L, Peri S, Kuo YM, Du F, Egleston BL, Ng JMY, Andrews AJ, Astsaturov I, Curran T, and Yang ZJ (2018). Statins synergize with Hedgehog pathway inhibitors for treatment of medulloblastoma. Clin. Cancer Res 24, 1375–1388. [PubMed: 29437795]

Hanahan D, and Weinberg RA (2011). Hallmarks of cancer: the next generation. Cell 144, 646–674. [PubMed: 21376230]

Hovestadt V, Jones DT, Picelli S, Wang W, Kool M, Northcott PA, Sultan M, Stachurski K, Ryzhova M, Warnatz HJ, et al. (2014). Decoding the regulatory landscape of medulloblastoma using DNA methylation sequencing. Nature 510, 537–541. [PubMed: 24847876]

Hovestadt V, Smith KS, Bihannic L, Filbin MG, Shaw ML, Baumgartner A, DeWitt JC, Groves A, Mayr L, Weisman HR, et al. (2019). Resolving medulloblastoma cellular architecture by single-cell genomics. Nature 572, 74–79. [PubMed: 31341285]

Ingham PW, and McMahon AP (2001). Hedgehog signaling in animal development: paradigms and principles. Genes Dev. 15, 3059–3087. [PubMed: 11731473]

Jin X, Kim LJY, Wu Q, Wallace LC, Prager BC, Sanvoranart T, Gimple RC, Wang X, Mack SC, Miller TE, et al. (2017). Targeting glioma stem cells through combined BMI1 and EZH2 inhibition. Nat. Med 23, 1352–1361. [PubMed: 29035367]

Kawauchi D, Robinson G, Uziel T, Gibson P, Rehg J, Gao C, Finkelstein D, Qu C, Pounds S, Ellison DW, et al. (2012). A mouse model of the most aggressive subgroup of human medulloblastoma. Cancer Cell 21, 168–180. [PubMed: 22340591]

Kim J, Tang JY, Gong R, Kim J, Lee JJ, Clemons KV, Chong CR, Chang KS, Fereshteh M, Gardner D, et al. (2010). Itraconazole, a commonly used antifungal that inhibits Hedgehog pathway activity and cancer growth. Cancer Cell 17, 388–399. [PubMed: 20385363]

Kuhar SG, Feng L, Vidan S, Ross ME, Hatten ME, and Heintz N (1993). Changing patterns of gene expression define four stages of cerebellar granule neuron differentiation. Development 117, 97–104. [PubMed: 8223263]

Leszczyniecka M, Roberts T, Dent P, Grant S, and Fisher PB (2001). Differentiation therapy of human cancer: basic science and clinical applications. Pharmacol. Ther 90, 105–156. [PubMed: 11578655]

Lewis PM, Gritli-Linde A, Smeyne R, Kottmann A, and McMahon AP (2004). Sonic hedgehog signaling is required for expansion of granule neuron precursors and patterning of the mouse cerebellum. Dev. Biol 270, 393–410. [PubMed: 15183722]

Li P, Lee EH, Du F, Gordon RE, Yuelling LW, Liu Y, Ng JM, Zhang H, Wu J, Korshunov A, et al. (2016). Nestin mediates Hedgehog pathway tumorigenesis. Cancer Res. 76, 5573–5583. [PubMed: 27496710]

Lin CY, Erkek S, Tong Y, Yin L, Federation AJ, Zapatka M, Haldipur P, Kawauchi D, Risch T, Warnatz HJ, et al. (2016). Active medulloblastoma enhancers reveal subgroup-specific cellular origins. Nature 530, 57–62. [PubMed: 26814967]

Liu Y, Yuelling LW, Wang Y, Du F, Gordon RE, O'Brien JA, Ng JMY, Robins S, Lee EH, Liu H, et al. (2017). Astrocytes promote medulloblastoma progression through Hedgehog secretion. Cancer Res. 77, 6692–6703. [PubMed: 28986380]

Manegold P, Lai KKY, Wu Y, Teo JL, Lenz HJ, Genyk YS, Pandol SJ, Wu K, Lin DP, Chen Y, et al. (2018). Differentiation therapy targeting the β-catenin/CBP interaction in pancreatic cancer. Cancers (Basel) 10, 10.

Mintz B, and Illmensee K (1975). Normal genetically mosaic mice produced from malignant teratocarcinoma cells. Proc. Natl. Acad. Sci. USA 72, 3585–3589. [PubMed: 1059147]

Miyata T, Maeda T, and Lee JE (1999). NeuroD is required for differentiation of the granule cells in the cerebellum and hippocampus. Genes Dev. 13, 1647–1652. [PubMed: 10398678]

Murone M, Rosenthal A, and de Sauvage FJ (1999). Sonic hedgehog signaling by the patched-smoothened receptor complex. Curr. Biol 9, 76–84. [PubMed: 10021362]

Nguyen L, Besson A, Heng JI, Schuurmans C, Teboul L, Parras C, Philpott A, Roberts JM, and Guillemot F (2006). p27kip1 independently promotes neuronal differentiation and migration in the cerebral cortex. Genes Dev. 20, 1511–1524. [PubMed: 16705040]

Northcott PA, Korshunov A, Pfister SM, and Taylor MD (2012). The clinical implications of medulloblastoma subgroups. Nat. Rev. Neurol 8, 340–351. [PubMed: 22565209]

Northcott PA, Robinson GW, Kratz CP, Mabbott DJ, Pomeroy SL, Clifford SC, Rutkowski S, Ellison DW, Malkin D, Taylor MD, et al. (2019). Medulloblastoma. Nat. Rev. Dis. Primers 5, 11. [PubMed: 30765705]

Oliver TG, Read TA, Kessler JD, Mehmeti A, Wells JF, Huynh TT, Lin SM, and Wechsler-Reya RJ (2005). Loss of patched and disruption of granule cell development in a pre-neoplastic stage of medulloblastoma. Development 132, 2425–2439. [PubMed: 15843415]

Packer RJ, and Hoffman EP (2012). Neuro-oncology: understanding the molecular complexity of medulloblastoma. Nat. Rev. Neurol 8, 539–540. [PubMed: 22986433]

Pan N, Jahan I, Lee JE, and Fritzsch B (2009). Defects in the cerebella of conditional Neurod1 null mice correlate with effective Tg(Atoh1-cre) recombination and granule cell requirements for Neurod1 for differentiation. Cell Tissue Res. 337, 407–428. [PubMed: 19609565]

Pei Y, Moore CE, Wang J, Tewari AK, Eroshkin A, Cho YJ, Witt H, Korshunov A, Read TA, Sun JL, et al. (2012). An animal model of MYC-driven medulloblastoma. Cancer Cell 21, 155–167. [PubMed: 22340590]

Pierce GB (1983). The cancer cell and its control by the embryo. Rous-Whipple Award lecture. Am. J. Pathol 113, 117–124. [PubMed: 6312802]

Pierce GB, and Wallace C (1971). Differentiation of malignant to benign cells. Cancer Res. 31, 127–134. [PubMed: 5545265]

Pomeroy SL, Sutton ME, Goumnerova LC, and Segal RA (1997). Neurotrophins in cerebellar granule cell development and medulloblastoma. J. Neurooncol 35, 347–352. [PubMed: 9440031]

Pöschl J, Lorenz A, Hartmann W, von Bueren AO, Kool M, Li S, Peraud A, Tonn JC, Herms J, Xiang M, et al. (2011). Expression of BARHL1 in medulloblastoma is associated with prolonged survival in mice and humans. Oncogene 30, 4721–4730. [PubMed: 21602885]

Romer JT, Kimura H, Magdaleno S, Sasai K, Fuller C, Baines H, Connelly M, Stewart CF, Gould S, Rubin LL, and Curran T (2004). Suppression of the Shh pathway using a small molecule inhibitor eliminates medulloblastoma in Ptc1(+/−)p53(−/−) mice. Cancer Cell 6, 229–240. [PubMed: 15380514]

Rudin CM, Hann CL, Laterra J, Yauch RL, Callahan CA, Fu L, Holcomb T, Stinson J, Gould SE, Coleman B, et al. (2009). Treatment of medulloblastoma with hedgehog pathway inhibitor GDC-0449. N. Engl. J. Med 361, 1173–1178. [PubMed: 19726761]

Salsano E, Pollo B, Eoli M, Giordana MT, and Finocchiaro G (2004). Expression of MATH1, a marker of cerebellar granule cell progenitors, identifies different medulloblastoma sub-types. Neurosci. Lett 370, 180–185. [PubMed: 15488319]

Sasaki K, Tamura S, Tachibana H, Sugita M, Gao Y, Furuyama J, Kakishita E, Sakai T, Tamaoki T, and Hashimoto-Tamaoki T (2000). Expression and role of p27(kip1) in neuronal differentiation of embryonal carcinoma cells. Brain Res. Mol. Brain Res 77, 209–221. [PubMed: 10837916]

Schüller U, Heine VM, Mao J, Kho AT, Dillon AK, Han YG, Huillard E, Sun T, Ligon AH, Qian Y, et al. (2008). Acquisition of granule neuron precursor identity is a critical determinant of progenitor cell competence to form Shh-induced medulloblastoma. Cancer Cell 14, 123–134. [PubMed: 18691547]

Tamayo-Orrego L, Wu CL, Bouchard N, Khedher A, Swikert SM, Remke M, Skowron P, Taylor MD, and Charron F (2016). Evasion of Cell Senescence Leads to Medulloblastoma Progression. Cell Rep. 14, 2925–2937. [PubMed: 26997276]

Taylor MD, Northcott PA, Korshunov A, Remke M, Cho YJ, Clifford SC, Eberhart CG, Parsons DW, Rutkowski S, Gajjar A, et al. (2012). Molecular subgroups of medulloblastoma: the current consensus. Acta Neuropathol. 123, 465–472. [PubMed: 22134537]

Tomayko MM, and Reynolds CP (1989). Determination of Subcutaneous Tumor Size in Athymic (Nude) Mice. Cancer Chemother Pharmacol. 24, 148–154. [PubMed: 2544306]

Ullrich NJ, and Pomeroy SL (2003). Pediatric brain tumors. Neurol. Clin 21, 897–913. [PubMed: 14743655]

Vanner RJ, Remke M, Gallo M, Selvadurai HJ, Coutinho F, Lee L, Kushida M, Head R, Morrissy S, Zhu X, et al. (2014). Quiescent sox2(+) cells drive hierarchical growth and relapse in sonic hedgehog subgroup medulloblastoma. Cancer Cell 26, 33–47. [PubMed: 24954133]

Vladoiu MC, El-Hamamy I, Donovan LK, Farooq H, Holgado BL, Sundaravadanam Y, Ramaswamy V, Hendrikse LD, Kumar S, Mack SC, et al. (2019). Childhood cerebellar tumours mirror conserved fetal transcriptional programs. Nature 572, 67–73. [PubMed: 31043743]

Vo BT, Li C, Morgan MA, Theurillat I, Finkelstein D, Wright S, Hyle J, Smith SMC, Fan Y, Wang YD, et al. (2017). Inactivation of Ezh2 upregulates Gfi1 and drives aggressive Myc-driven group 3 medulloblastoma. Cell Rep. 18, 2907–2917. [PubMed: 28329683]

Wang ZY, and Chen Z (2008). Acute promyelocytic leukemia: from highly fatal to highly curable. Blood 111, 2505–2515. [PubMed: 18299451]

Wechsler-Reya RJ, and Scott MP (1999). Control of neuronal precursor proliferation in the cerebellum by Sonic Hedgehog. Neuron 22, 103–114. [PubMed: 10027293]

Xenaki D, Martin IB, Yoshida L, Ohyama K, Gennarini G, Grumet M, Sakurai T, and Furley AJ (2011). F3/contactin and TAG1 play antagonistic roles in the regulation of sonic hedgehog-induced cerebellar granule neuron progenitor proliferation. Development 138, 519–529. [PubMed: 21205796]

Xie J, Murone M, Luoh SM, Ryan A, Gu Q, Zhang C, Bonifas JM, Lam CW, Hynes M, Goddard A, et al. (1998). Activating Smoothened mutations in sporadic basal-cell carcinoma. Nature 391, 90–92. [PubMed: 9422511]

Yang ZJ, Ellis T, Markant SL, Read TA, Kessler JD, Bourboulas M, Schüller U, Machold R, Fishell G, Rowitch DH, et al. (2008). Medulloblastoma can be initiated by deletion of Patched in lineage-restricted progenitors or stem cells. Cancer Cell 14, 135–145. [PubMed: 18691548]

Yauch RL, Dijkgraaf GJ, Alicke B, Januario T, Ahn CP, Holcomb T, Pujara K, Stinson J, Callahan CA, Tang T, et al. (2009). Smoothened mutation confers resistance to a Hedgehog pathway inhibitor in medulloblastoma. Science 326, 572–574. [PubMed: 19726788]

Yokota N, Aruga J, Takai S, Yamada K, Hamazaki M, Iwase T, Sugimura H, and Mikoshiba K (1996). Predominant expression of human zic in cerebellar granule cell lineage and medulloblastoma. Cancer Res. 56, 377–383. [PubMed: 8542595]

Yokota N, Mainprize TG, Taylor MD, Kohata T, Loreto M, Ueda S, Dura W, Grajkowska W, Kuo JS, and Rutka JT (2004). Identification of differentially expressed and developmentally regulated genes in medulloblastoma using suppression subtraction hybridization. Oncogene 23, 3444–3453. [PubMed: 15064731]

Zhang P, de Gooijer MC, Buil LC, Beijnen JH, Li G, and van Tellingen O (2015). ABCB1 and ABCG2 restrict the brain penetration of a panel of novel EZH2-Inhibitors. Int. J. Cancer 137, 2007–2018. [PubMed: 25868794]

Zhao H, Ayrault O, Zindy F, Kim JH, and Roussel MF (2008). Post-transcriptional down-regulation of Atoh1/Math1 by bone morphogenic proteins suppresses medulloblastoma development. Genes Dev. 22, 722–727. [PubMed: 18347090]

Highlights

- Medulloblastoma cell differentiation can resemble that of cerebellar neuronal progenitors
- Differentiated tumor cells permanently lose their tumorigenic capacity
- NeuroD1 drives the differentiation of medulloblastoma cells
- EZH2 inhibitors repress medulloblastoma growth by inducing tumor cell differentiation

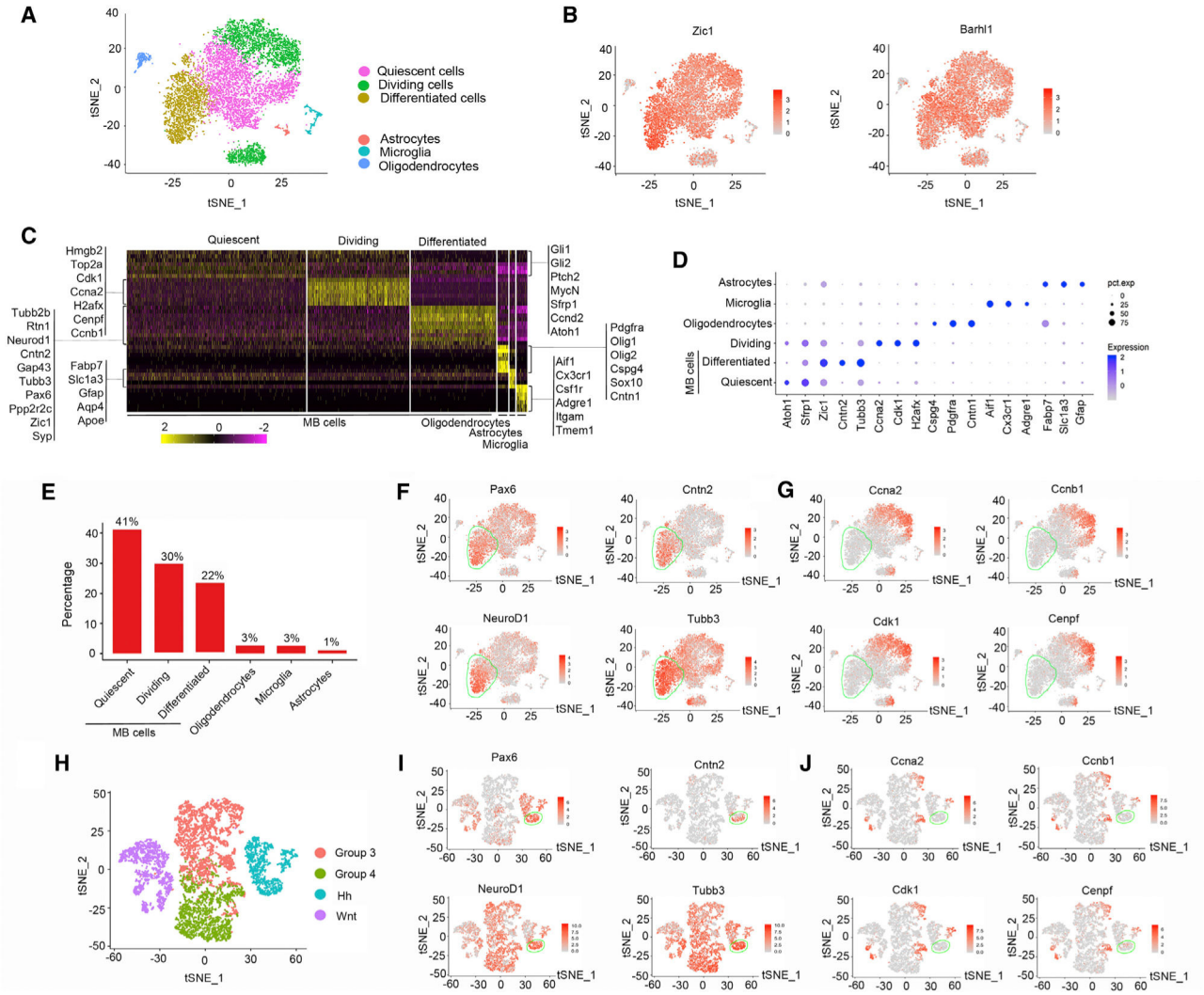

Figure 1. Tumor Cell Differentiation in Ptch1-Deficient MB

(A) tSNE plot showing cell clusters based on transcriptomes of cells isolated from MB in *Ptch1*$^{+/-}$ mice. Cell clusters are color coded.

(B) tSNE plots displaying the expression levels of *Zic1* and *Barhl1* in all cell clusters.

(C) Heatmap of single-cell data based on the tSNE plot. Columns represent individual cells, and rows represent genes.

(D) Dot plot showing the expression of marker genes in each cell clusters. The size of the dot reflects the percentage of cells expressing the gene. Expression levels are color coded.

(E) The percentage of each clusters in total cells isolated from MB.

(F and G) tSNE plots showing the expression of neuronal differentiation genes (F) and cell-cycle-associated genes (G) in all cell clusters.

(H) tSNE plot showing tumor groups based on transcriptomes of human MB cells. Tumor groups are color coded.

(I and J) tSNE plots showing the expression of neuronal differentiation genes (I) and cell-cycle-associated genes (J).

A green line circles the differentiated cell cluster in (F), (G), (I), and (J).

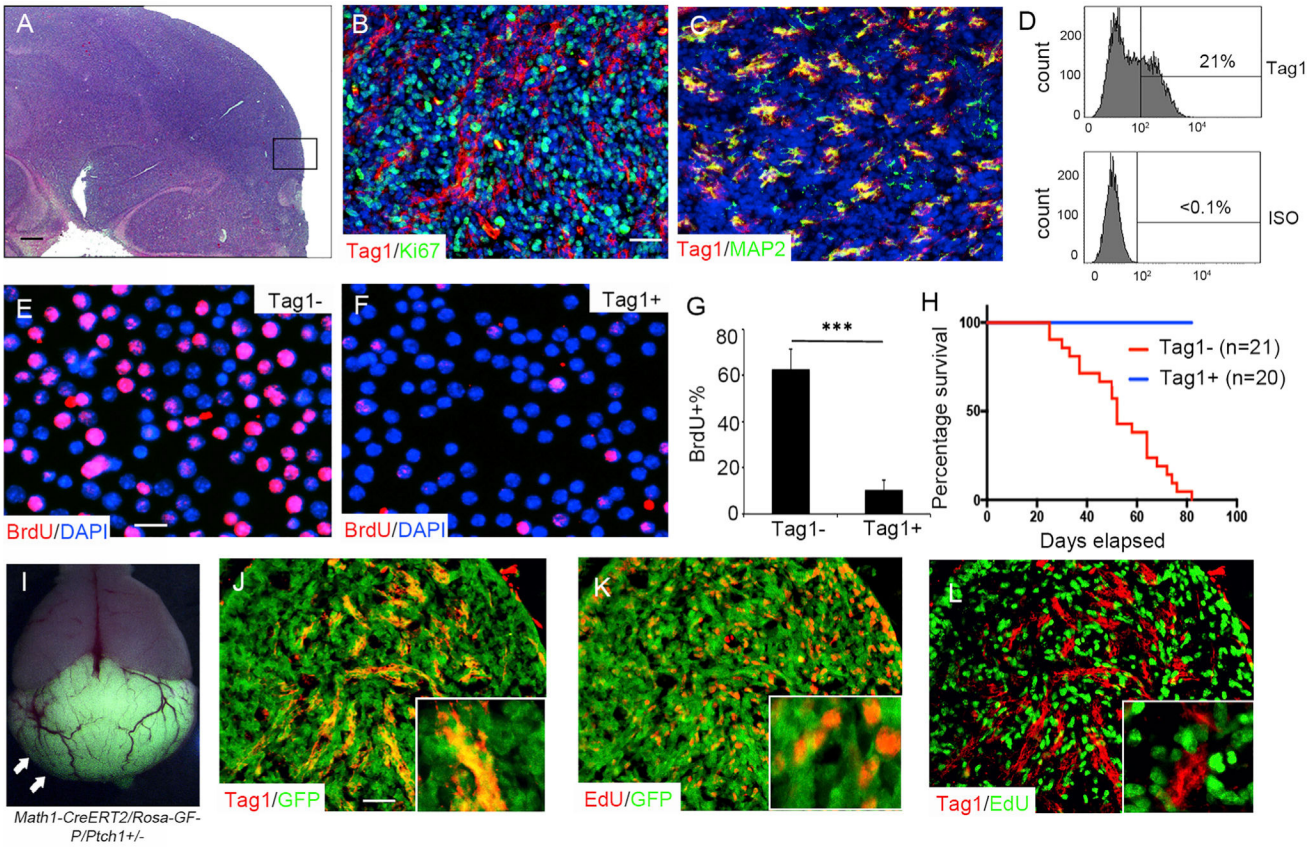

Figure 2. Differentiated MB Cells Are Not Tumorigenic

(A–C) MB tissues from *Ptch1*$^{+/-}$ mice were harvested for H&E staining (A) and immunostaining for Tag1/Ki67 (B) and Tag1/MAP2 (C). Tumor regions shown in (B) and (C) correlate the box region in (A).Scale bars,75 μm (A) and 50 μm (B and C).

(D) Histograms of tumor cells by flow cytometry after immunostaining with an antibody against Tag1 (top) or isotype control (bottom).

(E and F) Tag1^{-} (E) or Tag1^{+} tumor cells (F) purified from *Ptch1*$^{+/-}$ mice, were pulse labeled with BrdU for 2 h before immunocytochemistry (E and F). DAPI was used to counterstain cell nuclei. Scale bars, 25 μm.

(G) Percentage of BrdU^{+} cells in Tag1^{-} and Tag1^{+} tumor cells.

(H) Survival curves of *CB17/SCID* mice after intracranial transplantation of Tag1^{-} or Tag1^{+} MB cells (2 × 10^{5} cells/mouse) purified from *Ptch1*$^{+/-}$ mice by FACs.

(I) Whole-mount picture of a *Math1-CreER*^{T2}*/Rosa-GFP/Ptch1*$^{+/-}$ mice after tamoxifen treatment and injection with EdU at 2 h before sacrifice. Arrows point to the GFP-positive MB.

(J–L) MB tissue sections from *Math1-CreER*^{T2}*/R26-GFP/Ptch1*$^{+/-}$ mice after tamoxifen treatment were triple immunostained for Tag1, EdU, and GFP. The same section shows the expression of Tag1/GFP (J), EdU/GFP (K), and Tag1/EdU (L). Insets in (J) and (K) show high-power views. Scale bars, 50 μm.

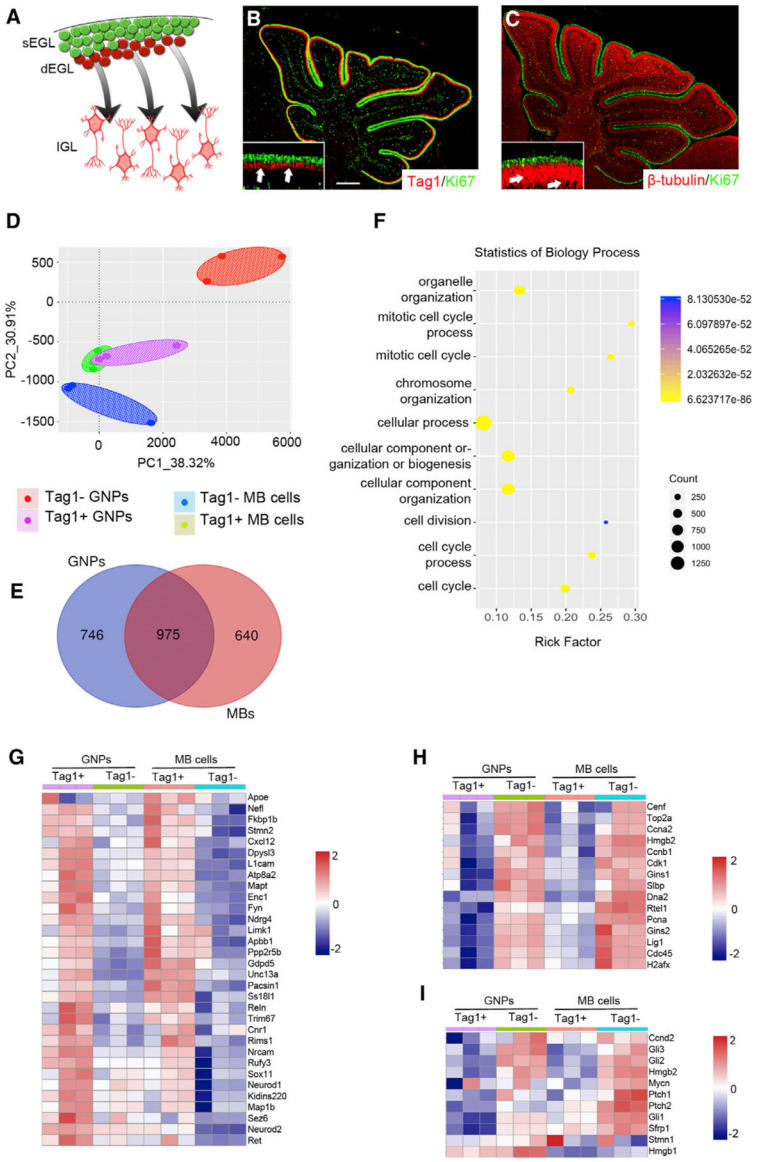

Figure 3. MB Cells Resemble GNPs in Their Differentiation

(A) Schematic of GNP differentiation in developing cerebellum. After completing their initiation proliferation in cerebellar sEGL, GNPs migrate through the dEGL to their final destination, the IGL.

(B and C) Cerebellar sections from wild-type cerebella at P6 were immunostained for Tag1/Ki67 (B) and βIII-tubulin/Ki67 (C). Insets show higher magnifications in (B) and (C). Arrows point to Tag1 expression (B) or βIII-tubulin expression (C). Scale bars, 100 μm.

(D) PCA of $Tag1^{-}$ tumor cells, differentiated tumor cells ($Tag1^{+}$), dividing GNPs ($Tag1^{-}$), and differentiated GNPs ($Tag1^{+}$) based on their transcriptomes.

(E) A Venn diagram showing the number of genes differentially expressed in dividing MB cells/GNPs and their differentiated counterparts.

(F) Gene Ontology (GO) analysis of differentially expressed genes based on biological processes.

(G–I) Heatmaps show the expression of genes associated with neuronal differentiation (G), cell cycle (H), and the Hh pathway (I) in tumor cells and GNPs.

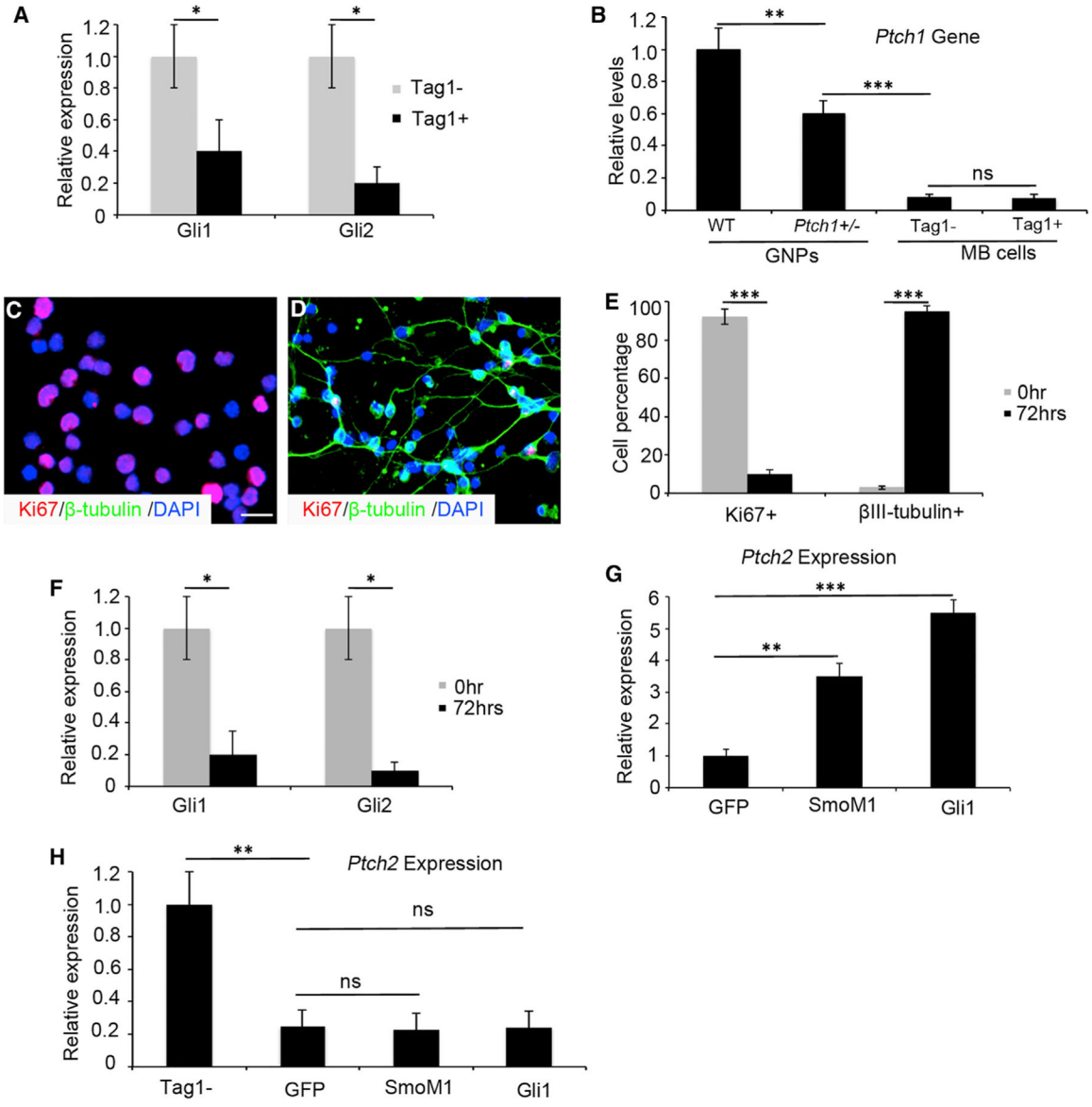

Figure 4. Differentiation Overrides Hh Signaling in MB Cells

(A) mRNA expressions of *Gli1* and *Gli2* in purified differentiated tumor cells (Tag1$^+$) and Tag1$^-$ tumor cells (Tag1$^-$) by qPCR.

(B) Relative abundance of *Ptch1* gene in GNPs and MB cells examined by conventional PCR.

(C and D) Purified Tag1$^-$ MB cells were harvested at 0 h (C) or 72 h (D) in culture to examine Ki67 and βIII-tubulin expressions by immunocytochemistry. DAPI was used to counterstain cell nuclei. Scale bars, 50 μm.

(E) Percentage of Ki67$^+$ and βIII-tubulin$^+$ cells among MB cells at 0 and 72 h.

(F) mRNA expression of *Gli1* and *Gli2* in cultured MB cells at 0 and 72 h.

(G) mRNA expression of *Ptch2* in cerebellar GNPs infected with a lentivirus carrying GFP control, *SmoM1*, or *Gli1*.

(H) mRNA expression of *Ptch2* in MB cells cultured for 72 h after overexpression of *SmoM1*, *Gli1*, or GFP control.

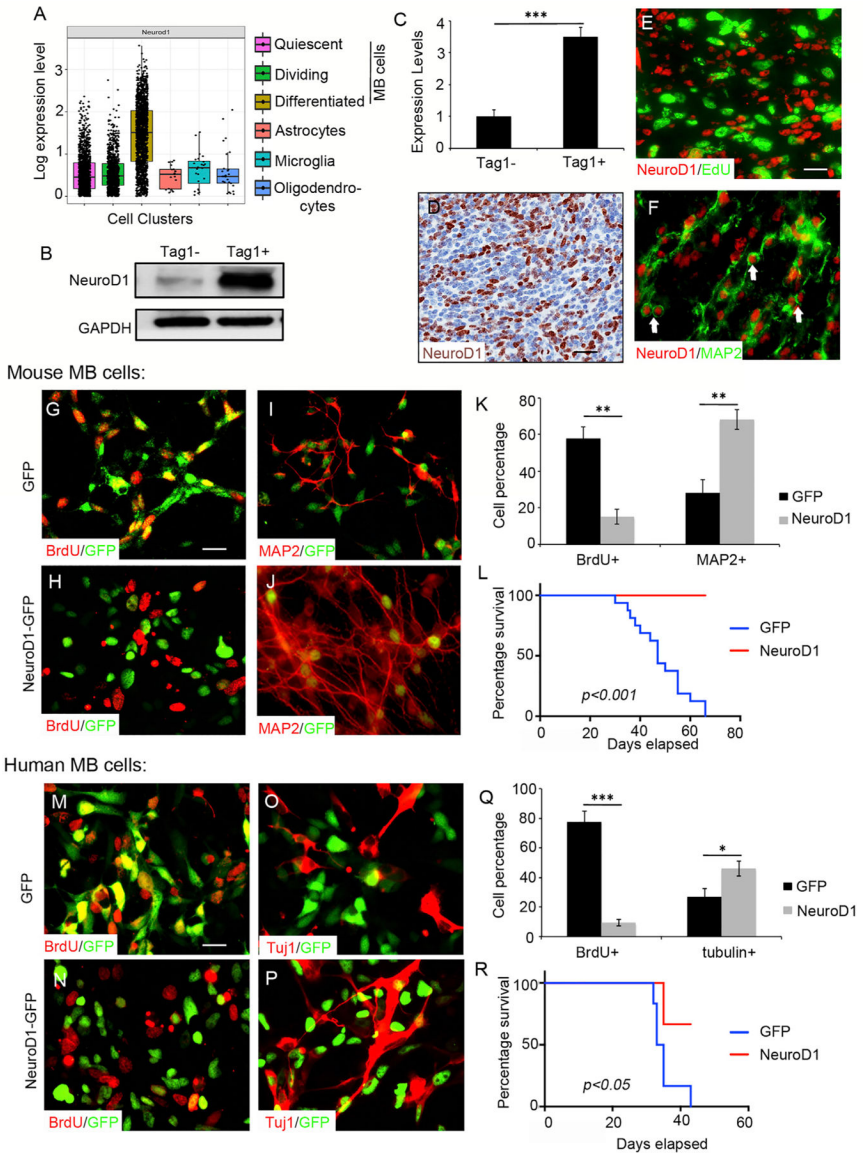

Figure 5. NeuroD1 Expression Stimulates MB Cell Differentiation

(A) Based on the transcriptomics of MB cells from scRNA-seq, a dot plot showing expression levels of *NeuroD1* mRNA in cell clusters in MB tissue. Each dot represents an individual cell.

(B and C) NeuroD1 protein (B) and mRNA (C) expression in $Tag1^+$ and $Tag1^-$ cells purified from MB tissue and examined by western blotting and qPCR, respectively.

(D) NeuroD1 protein expression in paraffin-embed sections of mouse MB by immunohistochemistry. Scale bar, 50 μm.

(E and F) NeuroD1/EdU (E) and NeuroD1/MAP2 (F) expression in MB sections examined by immunohistochemistry. Scale bars, 50 μm.

(G–K) MB cells after overexpressing *NeuroD1* (H and J) or *GFP* alone (G and I), were examined for BrdU (G and H) and MAP2 (I and J) expressions by immunocytochemistry. Scale bars, 25 μm (G-J).

(K) Percentage of $BrdU^+$ cells as well as $MAP2^+$ cells among infected MB cells (GFP^+).
(L) Survival curves of *CB17/SCID* mice after intracranial transplantation of MB cells with overexpression of *NeuroD1* or *GFP* alone.
(M–R) Human Hh-group MB cells infected with lentivirus encoding *GFP* (M and O) or *NeuroD1* (N and P) were pulsed with BrdU for 2 h before being harvested to examine BrdU and βIII-tubulin by immunocytochemistry. (Q) Percentages of $BrdU^+$ cells and βIII-$tubulin^+$ cells among infected MB cells (GFP^+). (R) Survival curves of *CB17/SCID* mice after intracranial injection of human MB cells with overexpression of *NeuroD1* (n = 6) or *GFP* alone (n = 6). Scale bars, 25 μm (M–P).

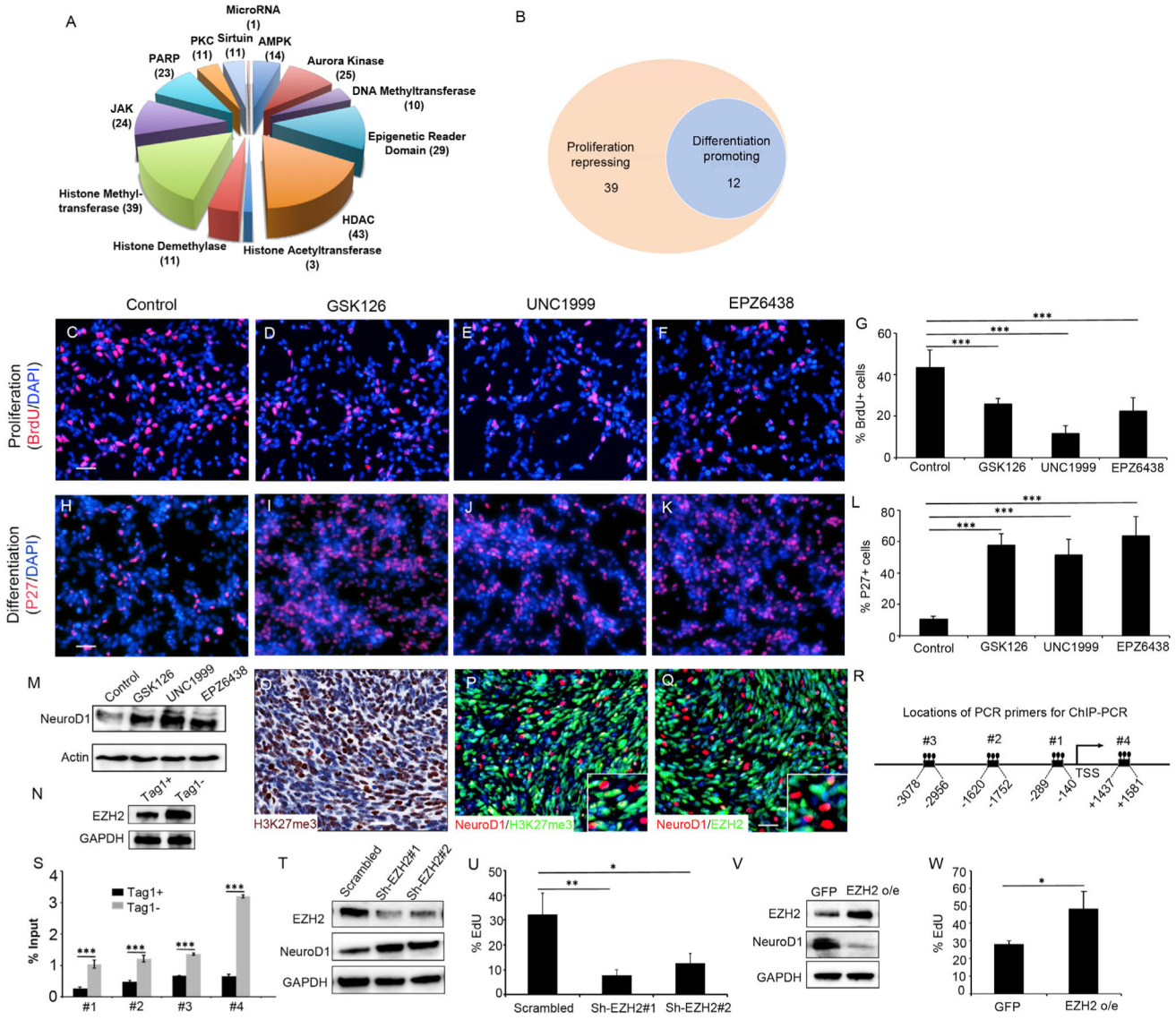

Figure 6. NeuroD1 Expression in MB Cells Was Repressed by H3K27me3

(A) Epigenetic compounds used for drug screening. The numbers in parentheses indicate the number of compounds in each category.

(B) Distribution of compounds in affecting tumor cell proliferation or differentiation.

(C–L) MB cells treated with DMSO (control, C and H), GSK126 (D and I), UNC1999 (E and J), or EPZ6438 (F and K) (all at 1 μM) for 48 h were collected to examine BrdU (C–F) or P27 (H–K) by immunocytochemistry. The percentage of $BrdU^+$ cells (G) or $P27^+$ cells (L) in the culture was quantified. DAPI was used to counterstain cell nuclei. Scale bars, 50 μm (C-F and H–K).

(M) NeuroD1 expression in MB cells after designated treatment, as examined by western blotting.

(N) EZH2 protein expression in purified $Tag1^+$ MB and $Tag1^-$ MB cells, as examined by western blotting.

(O) H3K27me3 protein expression in paraffin embedded MB tissue from *Ptch1*$^{+/-}$ mice, as examined by immunohistochemistry. Scale bar, 50 μm.
(P and Q) NeuroD1/H3K27me3 (P) and NeuroD1/EZH2 (Q) expression in frozen MB tissues from *Ptch1*$^{+/-}$ mice by immunohistochemistry. Insets show high-power views. Scale bars, 50 μm.
(R) A schematic showing locations of PCR primers used for detecting occupancy of H3K27me3 or H3K27ac on NeuroD1 promoter or enhancers.
(S) Enrichment of H3K27me3 on NeuroD1 loci in purified Tag1^{+} and Tag1^{-} MB cells.
(T–W) MB cells from *Ptch1*$^{+/-}$ mice were infected with shRNAs specific for EZH2 (Sh-EZH2#1 and Sh-EZH2#2) or scrambled shRNA, as well as with EZH2 or GFP alone for 48 h, and pulsed labeled with EdU for 2 h before collection. EZH2 and NeuroD1 proteins in infected cells were examined by western blotting (T and V). GAPDH was used as a loading control. The percentage of EdU^{+} cells among infected cells is quantified (U and W).

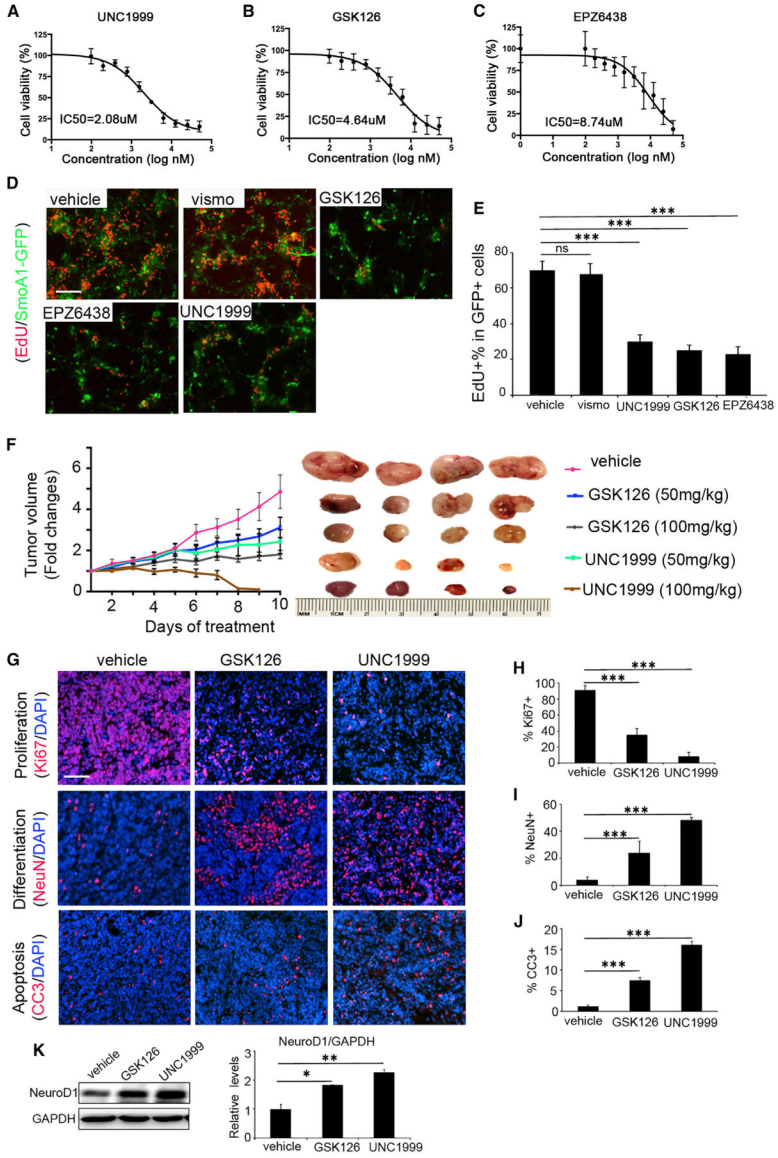

Figure 7. EZH2 Inhibitors Effectively Repress MB Growth

(A–C) IC_{50} values of UNC1999 (A), GSK126 (B), and EPZ6438 (C) in repressing MB proliferation, as examined by CCK8 assay.

(D and E) GNPs from P6 wild-type cerebella were infected with lentivirus encoding SmoA1-GFP and treated with vismodegib (400 nM), UNC1999 (2 μM), GSK126 (2 μM), or EPZ6438 (2 μM) for 48 h. GNPs after the treatment were examined for proliferation (EdU^+) by immunostaining (D). The percentage of EdU^+ cells in infected GNPs after treatment is quantified (E). Scale bar, 50 μm (D).

(F) Fold changes in the volume of subcutaneous MBs after the designated treatment, and the size of subcutaneous MB after drug treatment (right).

(G–K) Subcutaneous MB tissue after treatment with vehicle, GSK126 (100 mg/kg), or UNC1999 (100 mg/kg) was immunostained for Ki67, NeuN, or cleaved caspase-3 by immunohistochemistry (G). DAPI was used to counterstain cell nuclei. The percentage of

Ki67$^+$ cells (H), NeuN$^+$ cells (I), or CC3$^+$ cells (J) is quantified. NeuroD1 protein expression in MB tissue after the treatment was examined by western blotting and quantified (K). GAPDH was used as a loading control. Scale bar, 50 μm (G).

KEY RESOURCES TABLE

REAGENT or RESOURCE	SOURCE	IDENTIFIER
Antibodies		
Rabbit monoclonal anti-Ki67	Abcam	Cat#ab15580; RRID: AB_443209
Mouse monoclonal anti-NeuN	Abcam	Cat#ab104224; RRID: AB_10711040
Mouse monoclonal anti-beta III Tubulin	Abcam	Cat#ab78078; RRID: AB_2256751
Rabbit monoclonal anti-Cleaved Caspase-3	Cell Signaling Technology	Cat#9664; RRID: AB_2070042
Rabbit monoclonal anti-Microtubule-Associated Protein 2 (MAP2)	Millipore	Cat# AB5622; RRID: AB_91939
Rabbit Polyclonal anti-MEF2D	Abcam	Cat#ab32845; RRID:AB_776269
Mouse monoclonal anti-Neurofilament (NF-M)	DSHB	Cat#2H3; RRID:AB_531793
Mouse monoclonal anti-TAG-1	DSHB	Cat#4D7/TAG1; RRID:AB_531775
Rabbit monoclonal anti-ZIC1	Gift from Dr. Rosalind Segal	N/A
Mouse monoclonal anti-Neurod1	Abcam	Cat# ab60704; RRID: AB_943491
Chicken Polyclonal anti-GFP	Thermo Fisher Scientific	Cat#A10262; RRID:AB_2534023
Mouse monoclonal anti-BrdU	Sigma-Aldrich	Cat#B8434; RRID:AB_476811
Rabbit Polyclonal anti-HA	Sigma-Aldrich	Cat#H6908; RRID:AB_260070
Mouse monoclonal anti-p27	Santa Cruz Biotechnology	Cat#sc-1641; RRID:AB_628074
Rabbit monoclonal anti-Histone H3, Trimethyl (Lys27)	Cell Signaling Technology	Cat#9733; RRID:AB_2616029
Rabbit monoclonal anti-EZH2	Cell Signaling Technology	Cat#5246; RRID:AB_10694683
Rabbit monoclonal anti-Acetyl-Histone H3 (Lys27)	Cell Signaling Technology	Cat#8173; RRID:AB_10949503
Rabbit monoclonal anti-GAPDH	Cell Signaling Technology	Cat#2118; RRID:AB_561053
Biological Samples		
human MB PDX lines	Northwestern University	ICb-5610MB
human MB TMAs	The Children's Hospital of Philadelphia	Human MB collections
Chemicals, Peptides, and Recombinant Proteins		
Tamoxifen	Sigma-Aldrich	CAS#10540-29-1
UNC1999	CAYMAN	CAS#1431612-23-5
GSK126	CAYMAN	CAS#1346574-57-9
EPZ-6438	CAYMAN	CAS#1403254-99-8
Elacridar	MedChemExpress	CAS#143664-11-3
Epigenetics compound library	MedChemExpress	CAS#HY-L005
Critical Commercial Assays		
Cell Counting Kit-8	MedChemExpress	CAS#HY-K0301
EZ DNA Methylation-Gold Kit	Zymo Research	CAS#D5005
ChIP DNA Clean & Concentrator	Zymo Research	CAS#D5205
High-Capacity cDNA Reverse Transcription Kit	Thermo Fisher	CAS#4368814
SYBR Green PCR Master Mix	QIAGEN	CAS#330501
Deposited Data		
Single-cell RNaseq	This paper	Accession number:GSE150752

REAGENT or RESOURCE	SOURCE	IDENTIFIER
Single-cell RNaseq	Hovestadt et al., 2019	Accession number:GSE119926
Experimental Models: Organisms/Strains		
Mouse: Tg(Atoh1-cre/Esr1*)14Fsh/J (Also known as Math1-CreERT2)	Jackson Laboratory	https://www.jax.org/strain/007684
Mouse: Ptch1tm1Mps/J (Also known as Ptch+/−)	Jackson Laboratory	https://www.jax.org/strain/003081
Mouse: Tg(Atoh1-cre)1Bfri (Also known as Math1-Cre)	Jackson Laboratory	https://www.jax.org/strain/011104
Mouse: B6;129-Gt(ROSA)26Sortm2Sho/J (Also known as Rosa-GFP)	Jackson Laboratory	https://www.jax.org/strain/004077
Mouse: CB17/SCID	Fox Chase Cancer Center	N/A
Oligonucleotides		
QPCR-Gli1 F:5′CCAAGCCAACTTTATGTCAGGG3′	Integrated DNA Technologies	N/A
QPCR-Gli1R: 3′AGCCCGCTTCTTTGTTAATTTGA5′	Integrated DNA Technologies	N/A
QPCR-Gli2F: 5′GCCCTGGAGAGTCACCCTT3′	Integrated DNA Technologies	N/A
QPCR-Gli2R: 3′TGCACAGACCGGAGGTAGT5′	Integrated DNA Technologies	N/A
QPCR-Ptch2F: 5′GGCACTCACATCCGTCAACAAC3′	Integrated DNA Technologies	N/A
QPCR-Ptch2F: 3′GAAGACGAGCATTACCGCTGCA5′	Integrated DNA Technologies	N/A
QPCR-Neurod1 F: 5′CCTTGCTACTCCAAGACCCAGA3′	Integrated DNA Technologies	N/A
QPCR-Neurod1R: 3′TTGCAGAGCGTCTGTACGAAGG5′	Integrated DNA Technologies	N/A
QPCR-Neurod2F: 5′GCTACTCCAAGACGCAGAAGCT3′	Integrated DNA Technologies	N/A
QPCR-Neurod2R: 3′CACAGAGTCTGCACGTAGGACA5′	Integrated DNA Technologies	N/A
QPCR-MaptF: 5′CCTGAGCAAAGTGACCTCCAAG3′	Integrated DNA Technologies	N/A
QPCR-MaptR: 3′CAAGGAGCCAATCTTCGACTGG5′	Integrated DNA Technologies	N/A
QPCR-L1camF: 5′CTGCTGAAGACCACAACTCTCC3′	Integrated DNA Technologies	N/A
QPCR-L1camR: 3′CCGAAAGGTGTAGTGGACATAGG5′	Integrated DNA Technologies	N/A
ChIP-PCR-Neurod1#1F: 5′TCACCCCTCCCCAGAACTTTCCT3′	Integrated DNA Technologies	N/A
ChIP-PCR-Neurod1#1R: 3′AATAGGCAGGTCACGTGGTTCCC5′	Integrated DNA Technologies	N/A
ChIP-PCR-Neurod1#2F: 5′ACAATGCTCCTTGCTTGCTC3′	Integrated DNA Technologies	N/A
ChIP-PCR-Neurod1#2R: 3′GCATTGTGGGAGTTCTTTGG5′	Integrated DNA Technologies	N/A
ChIP-PCR-Neurod1#3F: 5′GTCTTGTCAGAACCTTGCCTTC3′	Integrated DNA Technologies	N/A
ChIP-PCR-Neurod1#3R: 3′CCCAGCATAGTTCTTGGATACC5′	Integrated DNA Technologies	N/A
ChIP-PCR-Neurod1#4F: 5′TGAACAGGGAGAGAGGCAAG3′	Integrated DNA Technologies	N/A
ChIP-PCR-Neurod1#4R: 3′CCATTTTGCAGTGGACTCCT5′	Integrated DNA Technologies	N/A